Astronomy & Astrophysics manuscript no. monit2
October 8, 2010
© ESO 2010

arXiv:1010.1461v1 [astro-ph.HE] 7 Oct 2010

X-ray monitoring of classical novae in the central region of M 31 II. Autumn and winter 2007/2008 and 2008/2009⋆

M. Henze[1], W. Pietsch[1], F. Haberl[1], M. Hernanz[2], G. Sala[3], D. Hatzidimitriou[4,5], M. Della Valle[6,7,8], A. Rau[1], D.H. Hartmann[9], and V. Burwitz[1]

[1] Max-Planck-Institut für extraterrestrische Physik, Giessenbachstraße, D-85748 Garching, Germany
email: mhenze@mpe.mpg.de
[2] Institut de Ciències de l'Espai (CSIC-IEEC), Campus UAB, Fac. Ciències, E-08193 Bellaterra, Spain
[3] Departament de Física i Enginyeria Nuclear, EUETIB (UPC-IEEC), Comte d'Urgell 187, 08036 Barcelona, Spain
[4] Department of Astrophysics, Astronomy and Mechanics, Faculty of Physics, University of Athens, Panepistimiopolis, GR15784 Zografos, Athens, Greece
[5] Foundation for Research and Technology Hellas, IESL, Greece
[6] European Southern Observatory (ESO), D-85748 Garching, Germany
[7] INAF-Napoli, Osservatorio Astronomico di Capodimonte, Salita Moiariello 16, I-80131 Napoli, Italy
[8] International Centre for Relativistic Astrophysics, Piazzale della Repubblica 2, I-65122 Pescara, Italy
[9] Department of Physics and Astronomy, Clemson University, Clemson, SC 29634-0978, USA

Received ? / Accepted ?

ABSTRACT

Context. Classical novae (CNe) represent the major class of supersoft X-ray sources (SSSs) in the central region of our neighbouring galaxy M 31.
Aims. We performed a dedicated monitoring of the M 31 central region with XMM-Newton and *Chandra* between Nov 2007 and Feb 2008 and between Nov 2008 and Feb 2009 respectively, in order to find SSS counterparts of CNe, determine the duration of their SSS phase and derive physical outburst parameters.
Methods. We systematically searched our data for X-ray counterparts of CNe and determined their X-ray light curves and spectral properties. Additionally, we determined luminosity upper limits for all previously known X-ray emitting novae which are not detected anymore and for all CNe in our field of view with optical outbursts between one year before the start of the X-ray monitoring (Oct 2006) and its end (Feb 2009).
Results. We detected in total 17 X-ray counterparts of CNe in M 31, only four of which were known previously. These latter sources are still active 12.5, 11.0, 7.4 and 4.8 years after the optical outburst. From the 17 X-ray counterparts 13 were classified as SSSs. In addition, we detected three known SSSs without a nova counterpart. Four novae displayed short SSS phases (< 100 d). Based on these results and previous studies we compiled a catalogue of all novae with SSS counterparts in M 31 known so far. We used this catalogue to derive correlations between the following X-ray and optical nova parameters: turn-on time, turn-off time, effective temperature (X-ray), t_2 decay time and expansion velocity of the ejected envelope (optical). Furthermore, we found a first hint for the existence of a difference between SSS parameters of novae associated with the stellar populations of the M 31 bulge and disk. Additionally, we conducted a Monte Carlo Markov Chain simulation on the intrinsic fraction of novae with SSS phase. This simulation showed that the relatively high fraction of novae without detected SSS emission might be explained by the inevitably incomplete coverage with X-ray observations in combination with a large fraction of novae with short SSS states, as expected from the WD mass distribution.
Conclusions. Our results confirm that novae are the major class of SSSs in the central region of M 31. The catalogue of novae with X-ray counterpart, mainly based on our X-ray monitoring, does contain valuable insight into the physics of the nova process. In order to verify our results with an increased sample further monitoring observations are needed.

Key words. Galaxies: individual: M 31 – novae, cataclysmic variables – X-rays: binaries – stars: individual: M31N 1996-08b, M31N 1997-11a, M31N 2001-10a, M31N 2003-08c, M31N 2004-01b, M31N 2004-05b, M31N 2007-02b, M31N 2007-06b, M31N 2007-10b, M31N 2007-11a, M31N 2007-12b, M31N 2008-05a, M31N 2008-05b, M31N 2008-06a

1. Introduction

This is the second of two papers analysing data from recent X-ray monitoring campaigns for classical novae in the central region of our neighbour galaxy M 31. In the first paper (Henze et al. 2010, hereafter Paper I) we presented the results of an earlier campaign from June 2006 to March 2007. Here we report our findings from the second and third monitoring seasons from November 2007 until February 2008 and from November 2008 until February 2009, respectively.

Classical novae (CNe) originate from thermonuclear explosions on the surface of white dwarfs (WDs) in cataclysmic binaries. Hydrogen-rich matter is transferred from the companion star to the WD. It accumulates on the surface of the WD until hydrogen ignition starts a thermonuclear runaway in the degenerate matter of the WD envelope. The resulting expansion of the hot envelope causes the brightness of the WD to rise by ∼ 12 magnitudes within a few days. Mass is ejected at high velocities (see Warner 1995; Hernanz 2005, and references therein).

⋆ Partly based on observations with XMM-Newton, an ESA Science Mission with instruments and contributions directly funded by ESA Member States and NASA

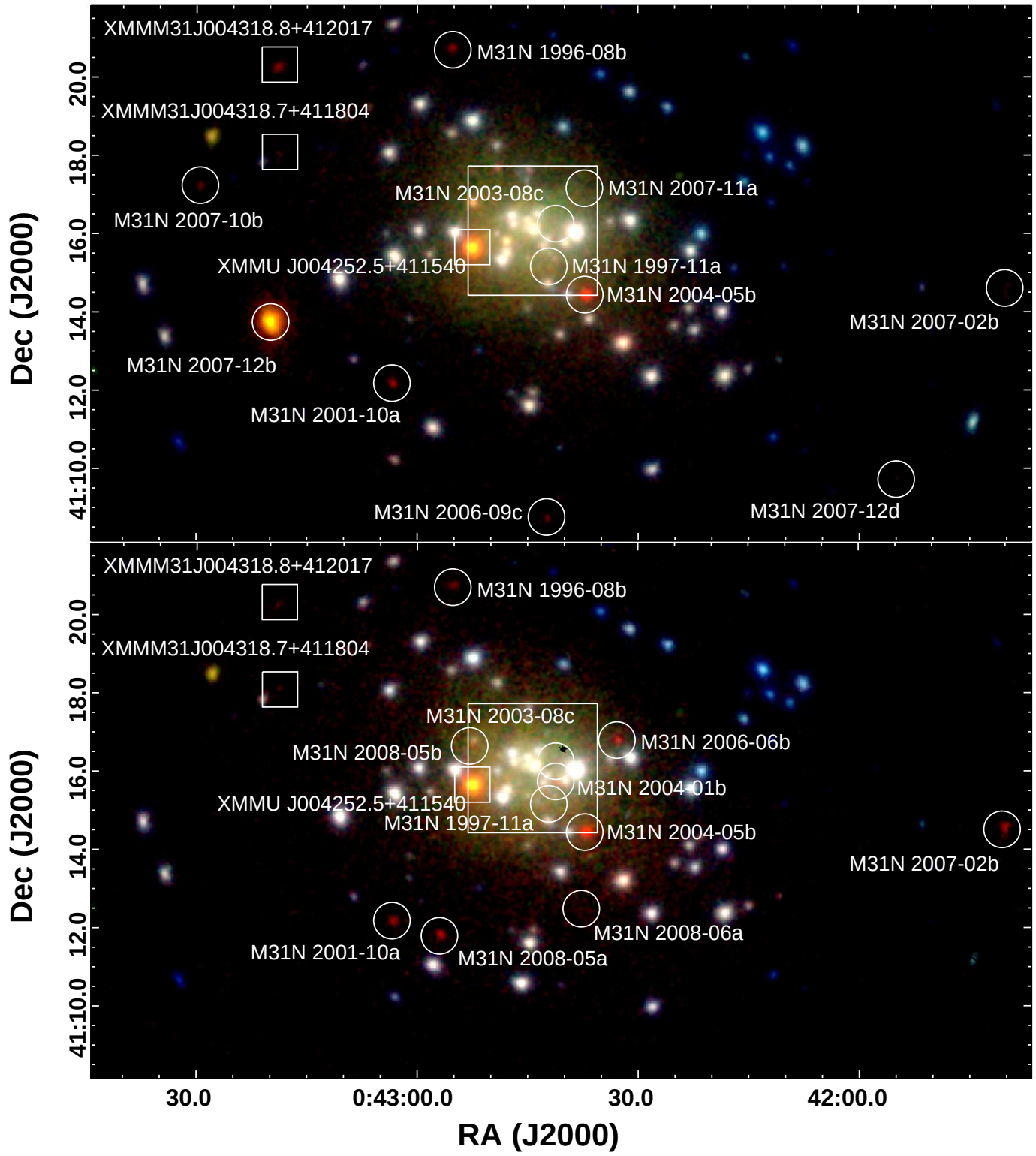

Fig. 1. Logarithmically-scaled, three colour XMM-Newton EPIC images of the central area of M 31 combining PN, MOS1 and MOS2 data of all five observations for 2007/8 (**top panel**) and 2008/9 (**bottom panel**). Red, green and blue show the (0.2 – 0.5) keV, (0.5 – 1.0) keV and (1.0 – 2.0) keV bands. SSS show up in red. The data in each colour band were binned in 2″x 2″pixels and smoothed using a Gaussian of FWHM 5″. The counterparts of optical novae detected in this work are marked with white circles. For M31N 1997-11a, M31N 2003-08c, M31N 2004-01b, M31N 2007-11a, M31N 2008-05b and M31N 2008-06a only the positions are designated, since they are not visible in these images but are detected in *Chandra* images. The non-nova SSSs detected in this work are marked with white boxes. The large white box includes the central region of M 31 which is shown as a *Chandra* composite in Fig. 2.

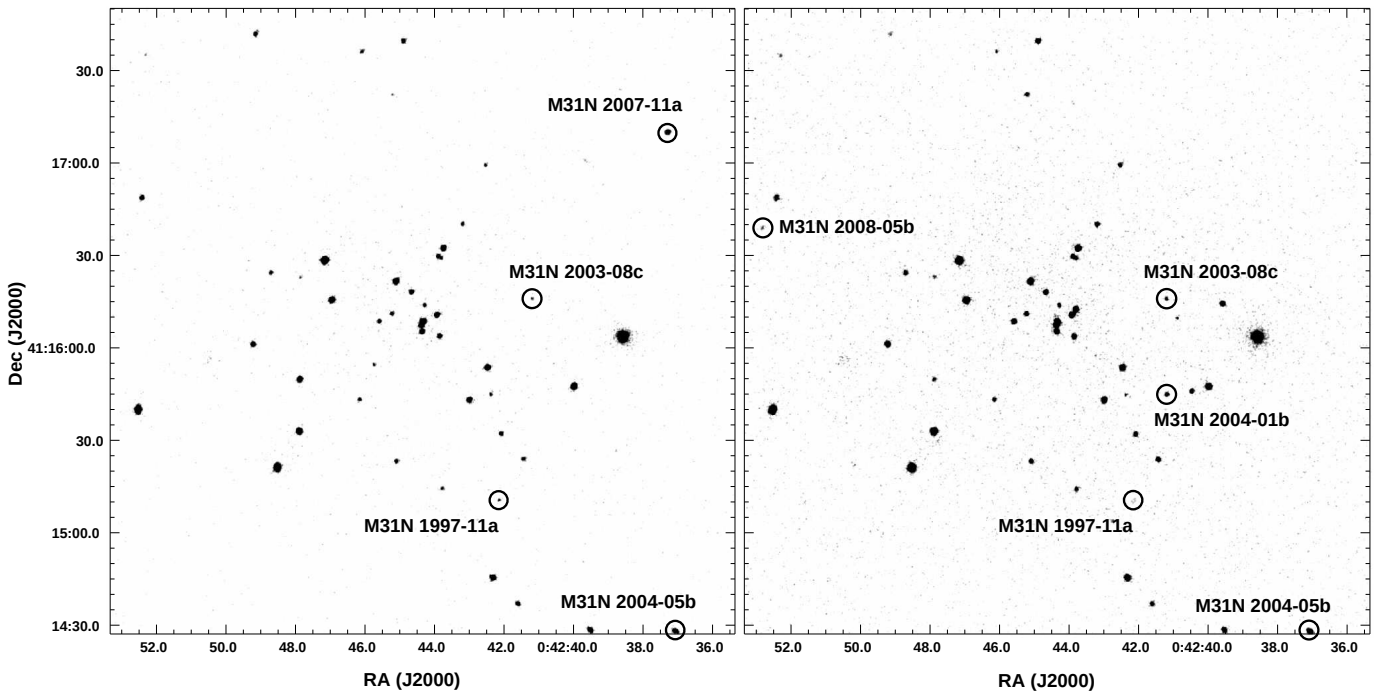

Fig. 2. Logarithmically-scaled *Chandra* HRC-I images of the innermost $3\farcm3 \times 3\farcm3$ of M 31 combining all observations of 2007/8 (**left panel**) and 2008/9 (**right panel**). The images have not been binned (HRC electronic pixel size = $0\farcs13$) but have been smoothed with a Gaussian of FWHM $0\farcs5$. The X-ray counterparts of novae in the field are marked with black circles.

However, a fraction of the hot envelope can remain in steady hydrogen burning on the surface of the WD (Starrfield et al. 1974; Sala & Hernanz 2005), powering a supersoft X-ray source (SSS) that can be observed directly, once the ejected envelope becomes sufficiently transparent (Starrfield 1989; Krautter 2002). In this paper, we define the term "turn-on of the SSS" from an observational point of view as the time when the SSS becomes visible to us, due to the decreasing opacity of the ejected material. This is not the same as the actual turn-on of the H-burning on the WD surface at the beginning of the thermonuclear runaway. The turn-off of the SSS, on the other hand, does not suffer from extinction effects and clearly marks the actual turn-off of the H-burning in the WD envelope and the disappearance of the SSS.

The class of SSSs was first characterised on the basis of ROSAT observations (Trümper et al. 1991; Greiner et al. 1991). These sources show extremely soft X-ray spectra, with little or no emission at energies above 1 keV, that can be described by equivalent blackbody temperatures of ∼15-80 eV (see Kahabka & van den Heuvel 1997, and references therein). It is well known that blackbody fits to SSS spectra are *not* a physically appropriate model. These fits produce in general too high values of $N_{\rm H}$ and too low temperatures, resulting in overestimated luminosities (see e.g. Greiner et al. 1991; Kahabka & van den Heuvel 1997, and references therein). A more realistic approach would be to use stellar atmosphere models that assume non-local thermodynamic equilibrium (NLTE) (see e.g. van Rossum & Ness 2010, and references therein). These models are still in development, but have been tested on bright Galactic CNe with promising results for static atmospheres (see e.g. Nelson et al. 2008b) and expanding atmospheres (see e.g. Petz et al. 2005). However, these models are more justified when interpreting high spectral resolution observations. SSSs in M 31 (distance 780 kpc; Holland 1998; Stanek & Garnavich 1998) are not bright enough to be observed with X-ray grating spectrometers. Furthermore, in the M 31 central region the source density is too high and the diffuse emission too strong to successfully apply grating spectroscopy for individual sources with the XMM-Newton RGS (Reflection Grating Spectrometer, den Herder et al. 2001) or the *Chandra* LETGS (Low-Energy Transmission Grating, Brinkman et al. 2000) or HETGS (High-Energy Transmission Grating, Canizares et al. 2005). Due to the low resolution and low signal-to-noise ratio of the XMM-Newton EPIC PN spectra analysed in this work, we decided to apply blackbody fits. In this way, we use the blackbody temperature as a simple parametrisation of the spectrum and can compare our results with earlier work (e.g. Pietsch et al. 2005a, 2007d), while keeping in mind the biases outlined above.

The duration of the SSS phase in CNe is related to the mass of H-rich matter that is *not* ejected and on the mass of the WD. Massive WDs have a strong surface gravity and theoretical models predict that they need less accreted matter to initiate the thermonuclear runaway (José & Hernanz 1998) and that they eject a smaller fraction of the accreted matter during the nova outburst (Yaron et al. 2005) compared to less massive WDs. Indeed, observations have found less massive ($\sim 2{\times}10^{-5}\ M_{\odot}$) ejecta associated with the brightest (very fast declining) novae. For slow novae the mass of the ejecta is about 10 times larger (Della Valle et al. 2002). In general, more massive WDs reach higher luminosities (Yaron et al. 2005) and retain less mass after the explosion, although this also depends on the accretion rate. Thus, the duration of the SSS state is inversely related to the mass of the WD, for a given hydrogen-mass fraction in the remaining envelope. On the other hand, the larger the hydrogen content, the longer the duration of the SSS state for a given WD mass (see Tuchman & Truran 1998; Sala & Hernanz 2005; Hachisu & Kato 2006).

Table 1. Observations of the M 31 monitoring.

Telescope/Instrument	ObsID	Exposure Time[a] [ks]				Start Date[b]	JD[b]	Offset[c]	
		PN	MOS1	MOS2	HRC-I	[UT]	2 450 000+	RA [″]	Dec [″]
2007/8									
Chandra HRC-I	8526				19.9	2007-11-07.63	4412.14	-0.3	0.3
Chandra HRC-I	8527				20.0	2007-11-17.76	4422.26	-0.3	0.3
Chandra HRC-I	8528				20.0	2007-11-28.79	4433.29	-0.2	0.2
Chandra HRC-I	8529				18.9	2007-12-07.57	4442.07	-0.3	0.1
Chandra HRC-I	8530				19.9	2007-12-17.49	4451.99	-0.3	0.1
XMM-Newton EPIC	0505720201	22.3	26.9	26.9		2007-12-29.57	4464.07	0.0	0.1
XMM-Newton EPIC	0505720301	20.4	26.4	26.4		2008-01-08.29	4473.79	0.0	0.1
XMM-Newton EPIC	0505720401	17.2	21.2	20.9		2008-01-18.63	4484.13	-0.3	0.1
XMM-Newton EPIC	0505720501	9.9	15.6	14.9		2008-01-27.94	4493.44	0.0	0.0
XMM-Newton EPIC	0505720601	15.1	20.7	20.7		2008-02-07.20	4503.75	0.0	0.3
2008/9									
Chandra HRC-I	9825				20.2	2008-11-08.34	4778.84	-0.3	0.2
Chandra HRC-I	9826				19.9	2008-11-17.14	4787.64	-0.4	0.3
Chandra HRC-I	9827				20.0	2008-11-28.24	4798.74	-0.3	0.3
Chandra HRC-I	9828				20.0	2008-12-07.41	4807.91	-0.4	0.1
Chandra HRC-I	9829				10.1	2008-12-18.02	4818.52	-0.5	0.0
Chandra HRC-I	10838				10.0	2008-12-18.49	4818.99	-0.4	0.1
XMM-Newton EPIC	0551690201	15.6	21.2	21.2		2008-12-30.14	4830.64	-0.1	0.1
XMM-Newton EPIC	0551690301	16.3	20.9	20.9		2009-01-09.26	4840.76	0.1	0.1
XMM-Newton EPIC	0551690401	6.1	9.9	10.0		2009-01-15.90	4847.40	0.1	0.0
XMM-Newton EPIC	0551690501	13.6	19.5	18.7		2009-01-27.31	4858.81	0.1	0.3
XMM-Newton EPIC	0551690601	12.7	5.5	5.5		2009-02-04.56	4867.06	-0.2	-0.1
Chandra HRC-I	10683				19.9	2009-02-16.90	4879.40	-0.5	0.1
Chandra HRC-I	10684				18.7	2009-02-26.17	4888.67	-0.5	0.1

Notes: [a]: Dead-time corrected; for XMM-Newton EPIC after screening for high background.
[b]: Start time of observations; for XMM-Newton EPIC the PN start time was used.
[c]: Offset of image WCS (world coordinate system) to the WCS of the catalogue by Kaaret (2002).

In turn, the transparency requirement mentioned above implies that the turn-on time is determined by the fraction of mass ejected in the outburst. X-ray light curves therefore provide important clues to the physics of the nova outburst, addressing the key question of whether a WD accumulates matter over time to become a potential progenitor for a type Ia supernova (SN-Ia). The duration of the SSS state provides the only direct indicator of the post-outburst hydrogen envelope mass in CNe. For massive WDs, the expected SSS duration is very short (< 100 d) (Tuchman & Truran 1998; Sala & Hernanz 2005).

Due to its proximity to the Galaxy and its moderate Galactic foreground absorption ($N_{\rm H} \sim 6.7 \times 10^{20}$ cm^{-2}, Stark et al. 1992), M 31 is a unique target for CN surveys which have been performed starting with the seminal work of Hubble (1929) (see also Shafter & Irby 2001; Henze et al. 2008b, and references therein). However, only recently nova monitoring programs for M 31 have been established that include fast data analysis and therefore provide the possibility to conduct follow-up spectroscopy (see e.g. Hatzidimitriou et al. 2007) and to confirm and classify CNe within the system of Williams (1992).

The advantages and disadvantages of X-ray surveys for CNe in M 31 compared to Galactic surveys (e.g. Orio et al. 2001; Ness et al. 2007) are similar to those of optical surveys. In our galaxy, the investigation of the entire nova population is hampered by the large area (namely the whole sky) to be scrutinised and by our unfavourable position, close to the Galactic Plane. As Ness et al. (2007) pointed out, the detectability of a SSS is highly dependent on its foreground absorption which attenuates the supersoft X-rays much more strongly than harder photons. Note that Orio et al. (2001) analysed 350 archival ROSAT observations and found SSS emission for only three Galactic novae. Galactic novae and SSSs can of course be studied in much greater detail than it is possible for M 31 objects, simply due to their proximity. But they have to be observed individually. Furthermore, determining the actual distance to a Galactic CN is by no means trivial. Observations of M 31 on the other hand, yield light curves of many CNe simultaneously and all of these objects are effectively at the same distance. Therefore, while Galactic sources are the ideal targets to examine the SSS emission of individual novae in detail, observations of M 31 allow us to study the "big picture" and provide insight into the CN population of a large spiral galaxy. Recently, Stiele et al. (2010) discussed SSSs in M 31 detected with ROSAT, XMM-Newton and *Chandra* and Orio et al. (2010) published a census of the SSS population of this galaxy.

M 31 has played a key role in nova population studies (e.g. Ciardullo et al. 1987; Capaccioli et al. 1989; Shafter & Irby 2001). The idea of two distinct optical nova populations was first introduced by Duerbeck (1990) and Della Valle et al. (1992) based on data on Galactic novae. They suggested that fast novae (time of decline by 2 magnitudes from maximum magnitude $t_2 \leq 12$ days) are mainly associated with the disk of the Galaxy or are concentrated close to the Galactic plane, whereas slower novae are mostly present in the bulge region of the Galaxy or at greater distances from the Galactic plane. Another argument

Table 2. Archival *Chandra* ACIS-I observations of the M 31 central region.

ObsID	Start Date [ks]	Exposure Time[a] [UT]
8195	2007-09-26.63	4.0
8186	2007-11-03.18	4.1
8187	2007-11-27.15	3.8
9520	2007-12-29.70	4.0
9529	2008-05-31.47	4.1
9522	2008-07-15.70	4.0
9523	2008-09-01.32	4.1
9524	2008-10-13.15	4.1
9521	2008-11-27.72	4.0
10551	2009-01-09.98	4.0
10552	2009-02-07.44	4.0
10553	2009-03-11.59	4.1

Notes: [a]: Dead-time corrected.

in favour of this idea came from Della Valle & Livio (1998), who reported systematic spectroscopic differences in the optical between Galactic bulge and disk novae. They found that novae that can be classified as "Fe II" novae in the system of Williams (1992) tend to be associated with the bulge of the Galaxy, whereas "He/N" novae mostly belong to the disk. According to Williams (1992), novae with prominent Fe II lines in the optical spectrum evolve more slowly with lower expansion velocities and lower levels of ionisation. On the other hand, novae with stronger lines of He and N have large expansion velocities and a rapid spectral evolution. These novae are often observed to also display strong Ne lines, which may point to a relatively massive ONe WD in the binary system (see e.g. Shafter & Quimby 2007). ONe WDs are believed to be initially more massive than CO WDs (José & Hernanz 1998) and therefore to have more massive progenitors. Therefore, a correlation of these objects with the younger (disk) stellar population seems plausible. There is an on-going controversy about which of the two populations dominates the nova rate in M 31 and the Galaxy (for an early overview see Hatano et al. 1997). In this paper, for the first time we study the differences between M 31 bulge and disk novae in the X-ray regime.

In Sect. 2, we describe our X-ray observations and data analysis. Results are presented in Sect. 3 and Sect. 4. An extensive discussion is given in Sect. 5.

2. Observations and data analysis

The X-ray data used in this work were obtained in a joint XMM-Newton/*Chandra* program (PI: W. Pietsch). We monitored the M 31 central region with five 20 ks XMM-Newton European Photon Imaging Camera (EPIC) observations following five 20 ks *Chandra* High-Resolution Camera Imaging Detector (HRC-I) observations each during autumn and winter 2007/8 and 2008/9, respectively. In 2008/9, the fifth *Chandra* observation was split in two parts of 10 ks duration each and two additional 20 ks HRC-I observations were performed in February 2009 after the XMM-Newton observations. All observations were pointed at the M 31 centre (RA: 00:42:44.33, Dec: +41:16:07.5; J2000).

The individual observations were separated by ten days, in contrast to the 40-day spacing in Paper I. We changed our monitoring strategy to account for a significant percentage of CNe in M 31 with short SSS phases found in our earlier work (see Pietsch et al. 2007d, hereafter PHS2007). The dates, observation identifications (ObsIDs) and dead-time corrected exposure times of the individual observations are given in Table 1. For the rest of the paper, 2007/8 and 2008/9 will indicate the corresponding monitoring campaign.

In the XMM-Newton observations, the EPIC PN and MOS instruments were operated in the full frame mode. We used the thin filter for PN and the medium filter for MOS.

Our data reduction and analysis techniques differ from the standard processing for both XMM-Newton EPIC and *Chandra* HRC-I and were described in detail in Paper I. The only change in this work was the update of all procedures to the most recent versions of the instrument dependent analysis software: XMMSAS (XMM-Newton Science Analysis System; Gabriel et al. 2004)[1] v9.0 and CIAO (Chandra Interactive Analysis of Observations; Fruscione et al. 2006)[2] v4.2. The statistical analysis described in Sect. 5 was performed using the R software environment[3]. For spectral fitting we used XSPEC v12.5.0. In all our spectral models we used the Tübingen-Boulder ISM absorption (`TBabs` in XSPEC) model together with the photoelectric absorption cross-sections from Balucinska-Church & McCammon (1992) and ISM abundances from Wilms et al. (2000). The statistical confidence ranges of parameters derived from spectral fits (e.g. blackbody temperature, $N_{\rm H}$) are 90% unless stated otherwise.

Additionally, during the time of both campaigns, there were twelve observations including the M 31 central region with *Chandra* ACIS-I and 62 observations with the *Swift* X-ray Telescope (XRT). These observations are summarised in Tables 2 (ACIS-I) and 3 (*Swift*) which list the ObsIDs, dead-time corrected exposure times and start dates, as well as the pointing distance to the M 31 centre for the *Swift* data. All ACIS-I observations were pointed directly at the M 31 centre. We checked all these observations for additional information on the novae found in our monitoring. In the ACIS-I data (see Table 2) none of the novae was detected. In the *Swift* XRT observations (see Table 3) three novae are visible. However, the information contained in these data has already been published by Henze et al. (2009a,b) and Bode et al. (2009) for novae M31N 2007-06b, M31N 2007-11a and M31N 2007-12b, respectively. Furthermore, there are no non-detections of SSS counterparts, that would result in additional constraints on their turn-on or turn-off time. The main reasons for this are (a) the temporal distribution of the observations and (b) the smaller field of view of the *Swift* XRT together with the fact that many observations were not pointed directly at the M 31 centre and therefore do not cover all nova positions (see Table 3). Therefore, the *Chandra* ACIS-I and *Swift* XRT data do not yield additional information on the novae discovered in this paper and will not be discussed further.

We also conducted a general search for SSSs in our XMM-Newton data, following the approach adopted by Pietsch et al. (2005a, hereafter PFF2005) using hardness ratios computed from count rates in energy bands 1 to 3 (0.2–0.5 keV, 0.5–1.0 keV, 1.0–2.0 keV) to classify a source. These authors defined hardness ratios and errors as

$$HR_i = \frac{B_{i+1} - B_i}{B_{i+1} + B_i} \text{ and } EHR_i = 2\frac{\sqrt{(B_{i+1}EB_i)^2 + (B_iEB_{i+1})^2}}{(B_{i+1} + B_i)^2} \ , \quad (1)$$

[1] http://xmm.esac.esa.int/external/xmm_data_analysis/
[2] http://cxc.harvard.edu/ciao/
[3] http://www.r-project.org

Table 3. Archival *Swift* XRT observations near the M 31 central region.

ObsID	Exp. time [ks]	Start Date [UT]	Distance[a] [arcmin]
00031017001	1.9	2007-11-18.39	14.8
00031017002	5.3	2007-11-19.26	15.4
00031028001/2	5.7	2007-11-24.20	2.9
00031027001	7.3	2007-11-24.33	13.7
00031028003/4	1.9	2007-11-27.01	3.8
00031028006	4.7	2007-11-30.02	2.6
00031027002	1.0	2007-12-02.64	13.1
00031028008	1.7	2007-12-02.97	2.6
00031027003	3.7	2007-12-03.24	14.1
00031017003	3.1	2007-12-13.01	16.6
00031017004	3.0	2007-12-14.02	15.9
00031017005	3.2	2007-12-15.02	16.4
00031027004	3.9	2007-12-16.77	14.5
00031017006	2.2	2007-12-20.24	16.4
00031017007	2.1	2007-12-22.38	16.6
00031017008	2.3	2007-12-24.32	16.3
00031027005	4.0	2007-12-30.01	15.9
00031017009	2.3	2007-12-30.15	16.6
00031017010	2.0	2008-01-03.43	17.6
00031017011	1.9	2008-01-06.24	15.9
00031017012	1.7	2008-01-09.99	16.9
00031027006	4.0	2008-01-13.74	15.2
00037717001	1.5	2008-05-26.04	29.2
00037718001	4.8	2008-05-26.29	11.6
00037719001	4.9	2008-05-26.70	2.3
00037720001	2.2	2008-05-26.96	13.8
00037721001	4.5	2008-05-28.11	27.7
00037720002	3.0	2008-05-28.84	15.6
00037725001	0.1	2008-07-04.51	16.9
00037724001	3.5	2008-07-04.60	23.3
00037711001	0.5	2008-07-06.13	24.9
00037712001	0.2	2008-07-06.53	14.0
00037713001	4.4	2008-07-06.80	15.5
00037714001	4.1	2008-07-07.07	25.0
00037725002	2.5	2008-07-09.41	14.3
00037717002	2.5	2008-07-09.62	26.3
00037712002	4.1	2008-07-20.45	13.4
00037711002	3.8	2008-07-20.79	25.0
00037726002	4.8	2008-07-22.06	14.5
00037727002	1.7	2008-07-24.20	25.7
00037727003	1.1	2008-07-26.48	26.3
00031255001	6.1	2008-08-21.30	2.4
00031255002	2.5	2008-08-28.67	2.6
00031255003	2.3	2008-09-04.22	1.5
00031255004	4.9	2008-09-06.59	2.9
00031255005	5.8	2008-09-11.47	0.8
00031255006	4.7	2008-09-25.50	2.1
00031255008	2.1	2008-10-14.73	1.2
00031255009	2.5	2008-10-15.14	1.6
00031255010	6.0	2008-10-21.63	1.0
00031255011	4.4	2008-10-28.65	1.2
00031283001	1.2	2008-12-07.07	1.5
00031283002	1.0	2008-12-08.14	1.9
00031283003	0.9	2008-12-09.01	1.9
00031283004	1.1	2008-12-10.08	2.2
00031283005	0.3	2008-12-11.02	2.0
00031283006	0.4	2008-12-12.02	2.3
00031283007	1.0	2008-12-13.22	1.8
00031283008	1.0	2008-12-14.03	2.7
00031283009	1.0	2008-12-15.17	1.7

Notes: [a]: Pointing distance from M 31 centre.

for $i = 1,2$, where B_i and EB_i denote count rates and corresponding errors in band i as derived by `emldetect`. PFF2005 classified sources as SSSs if they fulfil the conditions $HR_1 < 0.0$ and $HR_2 - EHR_2 < -0.4$. In this work we use the same criteria.

3. Results

In our two monitoring campaigns we detected in total 17 X-ray counterparts of CNe in M 31. In addition, 3 SSSs without a nova counterpart were found. The positions of all objects are indicated in Figs. 1 and 2, which show merged images from all observations in 2007/8 and 2008/9 for XMM-Newton and *Chandra*, respectively. X-ray measurements of all detected optical nova counterparts are given in Tables 4 and 5, whereas Tables 6, 7 and 8 present X-ray upper limits for known optical novae that were not detected. The Tables 4 – 8 contain the following information: the name, coordinates, and outburst date of the optical nova (taken from the online catalogue of PFF2005[4]), the distance between optical and X-ray source (if detected), the X-ray observation and its time lag with respect to the optical outburst, the unabsorbed X-ray luminosity or its upper limit, and comments. We give luminosities for the sources that were detected at least with a 2σ significance in the (0.2–10.0) keV band combining all EPIC instruments. Upper limits are 3σ, determined from the more sensitive EPIC PN camera if possible (see also PFF2005).

3.1. X-ray counterparts of optical novae in M 31 known before this work

Four of the 17 detected X-ray counterparts (see Table 4) were already seen in observations presented in Paper I: M31N 1996-08b, M31N 1997-11a, M31N 2001-10a and M31N 2004-05b. All of them had been previously detected in PHS2007 and are still visible at the end of the 2008/9 campaign.

Nova M31N 1996-08b remained active for 12.5 years after the optical discovery. Its X-ray spectrum did not change in 2007/8 and 2008/9 with respect to Paper I. In Fig. 3 we show the confidence contours of absorption column density and blackbody temperature for a combined spectral fit of all 2007/8 and 2008/9 spectra. Merging these data with the spectra obtained in Paper I we derived a new best fit effective temperature $kT = 21^{+8}_{-13}$ eV and an absorption $N_{\rm H} = (1.4^{+1.2}_{-0.8}) \times 10^{21}$ cm^{-2}. The values of both parameters are almost the same as in Paper I but the errors are significantly reduced. The luminosity of the source, given in Table 4, did not change significantly with respect to the 2006/7 observations reported in Paper I. Similarly, the X-ray light curve over 2007/8 and 2008/9 seems stable. Discrepancies between XMM-Newton and *Chandra* luminosities are likely to arise due to the differences of the generic spectral model used to compute the luminosities in Table 4 and the actual source spectrum. See Paper I for a discussion of this issue.

Nova M31N 1997-11a is situated close to the centre of M 31 and only detected in *Chandra* HRC-I data. The XMM-Newton images in this region suffer from source confusion. It was classified as a SSS in Paper I based on *Chandra* HRC-I hardness ratios and a comparison with *Chandra* ACIS-I upper limits. The X-ray light curve of the source shows a decline from an average $L_x = (7.6 \pm 0.8) \times 10^{36}$ erg s^{-1} in 2006/7 (Paper I) through $L_x = (3.2 \pm 0.4) \times 10^{36}$ erg s^{-1} in 2007/8 to $L_x = (0.6 \pm 0.2) \times 10^{36}$ erg s^{-1} in 2008/9 (see Table 4). However, note the increase of luminosity by a factor of two during observation 8529 which is interrupting the overall decline. In the last campaign, 11.0 years

[4] http://www.mpe.mpg.de/~m31novae/opt/m31/index.php

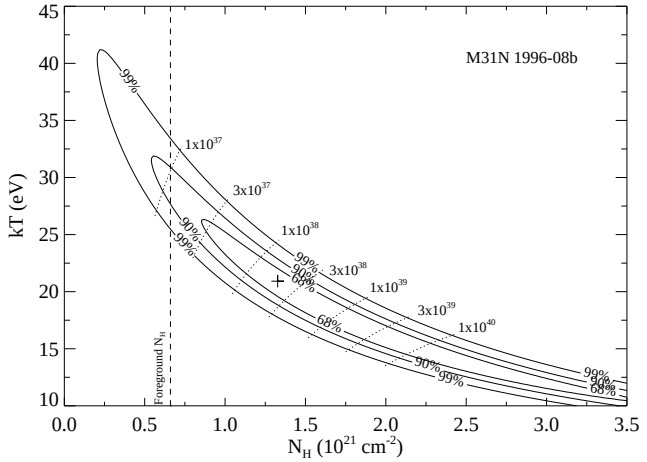

Fig. 3. Column density ($N_{\rm H}$) - temperature (kT) contours inferred from the fit to the XMM-Newton EPIC PN spectra of M31N 1996-08b for 2007/8 and 2008/9. Indicated are the formal best fit parameters (**cross**), the lines of constant X-ray luminosity (0.2-10.0 keV, **dotted lines**), and the Galactic foreground absorption (**dashed line**).

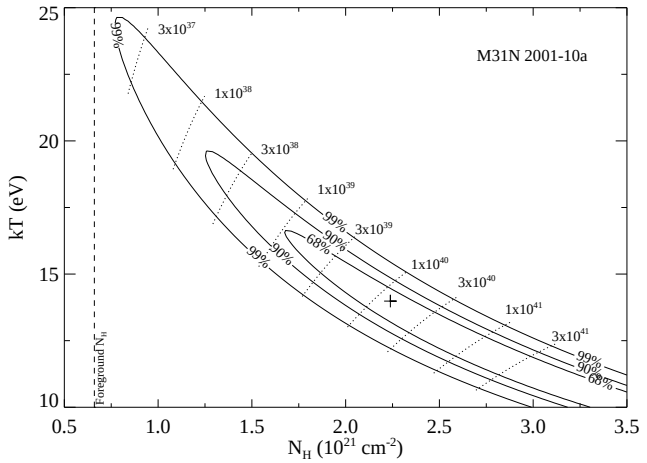

Fig. 4. Same as Fig. 3 for M31N 2001-10a for 2007/8 and 2008/9.

after the optical outburst, the source is so faint that it is only detected in the merged *Chandra* data.

Nova M31N 2001-10a is still active 7.4 years after the optical discovery. The best fit parameters for modelling the combined XMM-Newton 2007/8 and 2008/9 spectra are $kT = 14^{+5}_{-8}$ eV and $N_{\rm H}$ = (2.2 ± 0.5) ×10^{21} cm^{-2}. These values are not significantly different from the results presented in Paper I. A confidence contour plot for the fitted parameters is shown in Fig. 4. Fitting the spectra derived here together with the data from Paper I resulted in a slightly better constrained effective temperature $kT = 14^{+4}_{-7}$ eV. The X-ray luminosity averaged over the individual monitoring campaigns was constant within the errors at $L_x \sim 2.5{\times}10^{36}$ erg s^{-1} (XMM-Newton data). The X-ray light curve during the 2007/8 and 2008/9 campaigns did not vary significantly either (see Table 4). Differences between XMM-Newton and *Chandra* are again due to the generic spectrum which we used for converting count rates to fluxes and which does not take into account the low source temperature.

Nova M31N 2004-05b is the only truly bright SSS ($L \geq 10^{37}$ erg s^{-1}) among the four previously known counterparts.

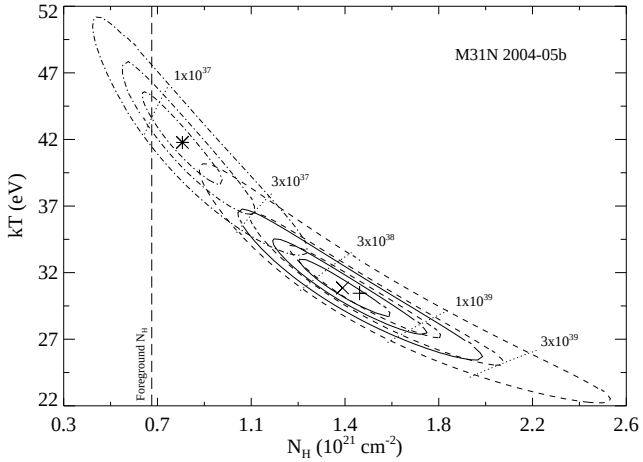

Fig. 5. Comparison of column density ($N_{\rm H}$) - temperature (kT) contours inferred from the individual fits to the XMM-Newton EPIC PN spectra of M31N 2004-05b for 2007/8 (solid lines) and 2008/9 (dash dotted lines). For reference, we also plot the confidence contours from Paper I (dashed lines). Best fit parameters are indicated with a plus sign (Paper I), a cross (2007/8) and an asterisk (2008/9). Further shown are the lines of constant X-ray luminosity (0.2-10.0 keV, dotted lines), and the Galactic foreground absorption (long dashed line).

The spectral evolution of this source is shown in Fig. 5. While the absorbed blackbody fit to the 2007/8 spectra is still compatible within the errors with the results from Paper I, the best fitting model for the 2008/9 spectra differs from the 2007/8 campaign at the 90% confidence level. This difference is illustrated in Fig. 5 and does manifest itself in significantly different best fit temperature and absorption: 2007/8: kT = (31 ± 4) eV, $N_{\rm H}$ = $(1.4^{+0.3}_{-0.2})$ ×10^{21} cm^{-2}; 2008/9: kT = (42 ± 6) eV, $N_{\rm H}$ = $(0.8^{+0.3}_{-0.2})$ ×10^{21} cm^{-2}. The X-ray light curve of M31N 2004-05b during 2007/8 (see Table 4) was relatively stable with similar luminosity as measured in 2006/7 (see Paper I). The 2008/9 luminosities might be slightly lower than those in 2007/8, but the effect is not significant and might be due to the spectral changes that the source is experiencing. Additionally, there was a strong increase in luminosity by a factor of about two in observation 8527, with respect to previous and subsequent observations (see Table 4).

3.2. X-ray counterparts of optical novae in M 31 newly discovered in this work

In total, 13 sources were detected for the first time in the observations of the campaigns presented here (see Table 5). The following three new sources exhibit extraordinary properties and were already discussed in detail in earlier work: M31N 2007-06b was the first nova in a M 31 globular cluster (Henze et al. 2009a). M31N 2007-11a had a well documented, very short SSS phase (Henze et al. 2009b). M31N 2007-12b was discussed for its X-ray light curve variability in Pietsch et al. (2010, in prep.) and Orio et al. (2010). The possibility that it is a recurrent nova was examined in Bode et al. (2009).

3.2.1. M31N 2003-08c

The optical nova was discovered by Fiaschi et al. (2003) on 2003-10-16 and spectroscopically confirmed by di Mille et al. (2003). A faint ($L_x \sim 3.5 \times 10^{36}$ erg s^{-1}) X-ray counterpart first showed up in the *Chandra* observations of 2007/8 (see Table 5).

Table 4. XMM-Newton and *Chandra* measurements of M 31 optical nova candidates known from Paper I and still detected here.

Optical nova candidate			X-ray measurements				
Name M31N	RA (h:m:s)[a] Dec (d:m:s)[a]	MJD[b] (d)	D[c] ($''$)	Observation[d] ID	Δt[e] (d)	L_X^f (10^{36} erg s^{-1})	Comment[g]
1996-08b	0:42:55.20 41:20:46.0	50307.0	0.8	mrg1 (HRC-I)	4104.6	4.1 ± 0.7	SSS
			1.2	0505720201 (EPIC)	4156.6	2.5 ± 0.5	
			1.3	0505720301 (EPIC)	4166.3	2.4 ± 0.4	
			1.8	0505720401 (EPIC)	4176.6	2.5 ± 0.6	
			0.5	0505720501 (EPIC)	4185.9	2.4 ± 0.7	
			2.2	0505720601 (EPIC)	4196.2	2.8 ± 0.6	
			0.5	mrg2 (HRC-I)	4471.3	3.9 ± 0.6	
			2.3	0551690201 (EPIC)	4523.1	2.3 ± 0.5	
			2.3	0551690301 (EPIC)	4533.3	1.6 ± 0.5	
				0551690401 (EPIC)	4539.9	< 4.7	
				0551690501 (EPIC)	4551.3	< 3.9	
			1.2	0551690601 (EPIC)	4559.6	2.5 ± 1.3	
1997-11a	0:42:42.13 41:15:10.5	50753.0	0.3	8526 (HRC-I)	3658.6	3.5 ± 0.8	SSS-HR
			0.4	8527 (HRC-I)	3668.8	3.4 ± 0.8	
			0.4	8528 (HRC-I)	3679.8	2.3 ± 0.8	
			0.5	8529 (HRC-I)	3688.6	6.0 ± 1.4	
			0.5	8530 (HRC-I)	3698.5	3.0 ± 0.9	
			0.5	mrg2 (HRC-I)	4025.3	0.6 ± 0.2	
2001-10a	0:43:03.31 41:12:11.5	52186.0	1.1	8526 (HRC-I)	2225.6	13.3 ± 2.2	SSS
			1.0	8527 (HRC-I)	2235.8	10.4 ± 1.9	
			1.5	8528 (HRC-I)	2246.8	9.9 ± 1.9	
			1.9	8529 (HRC-I)	2255.6	9.8 ± 1.9	
				8530 (HRC-I)	2265.5	< 9.8	
			1.0	0505720201 (EPIC)	2277.6	2.6 ± 0.4	
				0505720301 (EPIC)	2287.3	< 4.8	
			0.7	0505720401 (EPIC)	2297.6	2.7 ± 0.6	
			1.6	0505720501 (EPIC)	2306.9	3.4 ± 0.9	
			1.8	0505720601 (EPIC)	2317.2	3.6 ± 0.7	
			1.5	9825 (HRC-I)	2592.3	7.0 ± 1.8	
			2.1	9826 (HRC-I)	2601.1	8.1 ± 1.7	
			0.6	9827 (HRC-I)	2612.2	11.3 ± 2.2	
			0.3	9828 (HRC-I)	2621.4	10.8 ± 2.1	
			0.9	9829 (HRC-I)	2632.0	11.9 ± 3.4	
				10838 (HRC-I)	2632.5	< 20.4	
			0.7	0551690201 (EPIC)	2644.1	3.6 ± 0.6	
			1.7	0551690301 (EPIC)	2654.3	3.7 ± 0.7	
				0551690401 (EPIC)	2660.9	< 6.1	
				0551690501 (EPIC)	2672.3	< 4.0	
			1.1	0551690601 (EPIC)	2680.6	3.4 ± 0.9	
			1.4	10683 (HRC-I)	2692.9	7.3 ± 1.7	
				10684 (HRC-I)	2702.2	< 11.8	

Due to the position of the source close to the M 31 centre, our XMM-Newton data suffer from source confusion and can only provide luminosity upper limits that are larger than the measured luminosities inferred from *Chandra*. For Table 10 we adopt as turn-on time of the source the midpoint between the last observation from Paper I and the first *Chandra* observation in 2007/8. The light curve of the nova counterpart was variable by at least a factor of two over the course of 2007/8 and 2008/9 campaigns. The source was still detected in the last observation of 2008/9.

3.2.2. M31N 2004-01b

The optical nova candidate was discovered in the WeCAPP survey (Riffeser et al. 2001) on 2004-01-01 (see also PHS2007). An X-ray counterpart with an average luminosity $L_x = (6.1 \pm 0.5) \times 10^{36}$ erg s^{-1} was found in the *Chandra* data of 2008/9. This object was not detected in the *Chandra* data of the 2007/8 campaign with an upper limit of $L_x < 1.6 \times 10^{36}$ erg s^{-1} in observation 8530 (see Table 5). The turn-on time of the source given in Table 10 was assumed to be the midpoint between the observations 8530 and 9825. Because the source is located close to the M 31 centre, source confusion prevented XMM-Newton from detecting it. Towards the end of the 2008/9 campaign the luminosity of the source increased significantly up to $L_x = (11.1 \pm 1.6) \times 10^{36}$ erg s^{-1} in the second last *Chandra* observation.

Table 4. continued.

Optical nova candidate			X-ray measurements				
Name M31N	RA (h:m:s)[a] Dec (d:m:s)[a]	MJD[b] (d)	D^c ($''$)	Observation[d] ID	Δt^e (d)	L_X^f (10^{36} erg s^{-1})	Comment[g]
2004-05b	0:42:37.04	53143.0	0.4	8526 (HRC-I)	1268.6	20.9 ± 2.3	SSS
	41:14:28.5		0.4	8527 (HRC-I)	1278.8	47.9 ± 6.0	
			0.3	8528 (HRC-I)	1289.8	21.5 ± 2.6	
			0.3	8529 (HRC-I)	1298.6	24.8 ± 2.9	
			0.3	8530 (HRC-I)	1308.5	31.4 ± 3.4	
			1.4	0505720201 (EPIC)	1320.6	21.9 ± 0.9	
			1.2	0505720301 (EPIC)	1330.3	20.0 ± 0.9	
			1.1	0505720401 (EPIC)	1340.6	21.6 ± 1.0	
			1.2	0505720501 (EPIC)	1349.9	21.4 ± 1.3	
			1.0	0505720601 (EPIC)	1360.2	16.7 ± 1.0	
			0.3	9825 (HRC-I)	1635.3	19.5 ± 2.2	
			0.4	9826 (HRC-I)	1644.1	17.9 ± 2.2	
			0.4	9827 (HRC-I)	1655.2	25.4 ± 2.8	
			0.4	9828 (HRC-I)	1664.4	21.3 ± 2.6	
			0.4	9829 (HRC-I)	1675.0	19.9 ± 3.0	
			0.4	10838 (HRC-I)	1675.5	26.6 ± 3.9	
			1.2	0551690201 (EPIC)	1687.1	18.4 ± 1.0	
			0.8	0551690301 (EPIC)	1697.3	16.5 ± 1.0	
			0.6	0551690401 (EPIC)	1703.9	16.7 ± 1.9	
			1.2	0551690501 (EPIC)	1715.3	17.0 ± 1.0	
			0.6	0551690601 (EPIC)	1723.6	16.7 ± 1.2	
			0.7	10683 (HRC-I)	1735.9	33.9 ± 4.2	
			0.5	10684 (HRC-I)	1745.2	36.7 ± 4.6	

Notes: [a]: RA, Dec are given in J2000.0; [b]: Modified Julian Date of optical outburst; MJD = JD - 2 400 000.5; [c]: Distance in arcsec between optical and X-ray source; [d]: mrg1/2 (HRC-I/EPIC) indicates merged data of all HRC-I/EPIC observations during 2007/8 or 2008/9, mrg3 (HRC-I) indicates merged data of the *Chandra* observations 9829 and 10838 (taken on the same day) ; [e]: Time after observed start of optical outburst; [f]: unabsorbed luminosity in 0.2–10.0 keV band assuming a 50 eV blackbody spectrum with Galactic foreground absorption (luminosity errors are 1σ, upper limits are 3σ); [g]: SSS or SSS-HR indicate X-ray sources classified as supersoft based on XMM-Newton spectra or *Chandra* hardness ratios, respectively

3.2.3. M31N 2006-06b

The optical nova candidate was discovered independently by Ries (2006) and K. Hornoch[5] on 2006-06-06. Both authors report evidence pointing towards a slowly rising nova. An X-ray counterpart was detected in the first 2008/9 observation. Nothing was found at this position in the 2007/8 campaign, with an upper limit of $L_x < 1.6 \times 10^{36}$ erg s^{-1} in XMM-Newton observation 0505720601 (see Table 5). The source was visible in XMM-Newton and *Chandra* data until the end of the 2008/9 campaign with an average luminosity $L_x = (3.6 \pm 0.3) \times 10^{36}$ erg s^{-1} in *Chandra* data. The source luminosity was increasing significantly during the time span of the monitoring. The turn-on time given in Table 10 is estimated as the midpoint between the observations 0505720601 and 9825.

We fitted the XMM-Newton EPIC PN spectrum of the source with an absorbed blackbody model. The resulting confidence contours for absorption column density and blackbody temperature are shown in Fig. 6. This source can clearly be classified as a SSS. Since the best fit $N_{\rm H}$ is smaller than the foreground absorption, we estimated an effective temperature $kT = 33^{+4}_{-3}$ eV for the foreground $N_{\rm H}$ (6.7×10^{21} cm^{-2}) from Fig. 6.

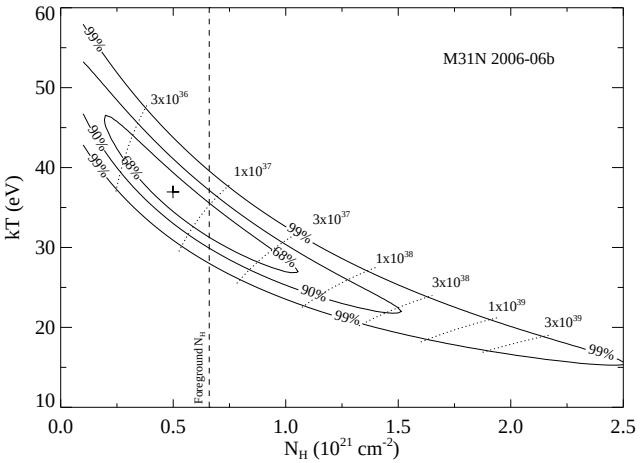

Fig. 6. Same as Fig. 3 for M31N 2006-06b in 2008/9.

3.2.4. M31N 2006-09c

The optical nova was discovered independently by K. Itagaki[6] and Quimby (2006) on 2006-09-18. Shafter et al. (2006) classified it as a Fe II nova. A faint ($L_x \lesssim 3.0 \times 10^{36}$ erg s^{-1}) X-ray

[5] see http://www.cfa.harvard.edu/iau/CBAT_M31.html#2006-06b

[6] see http://www.cfa.harvard.edu/iau/CBAT_M31.html#2006-09c

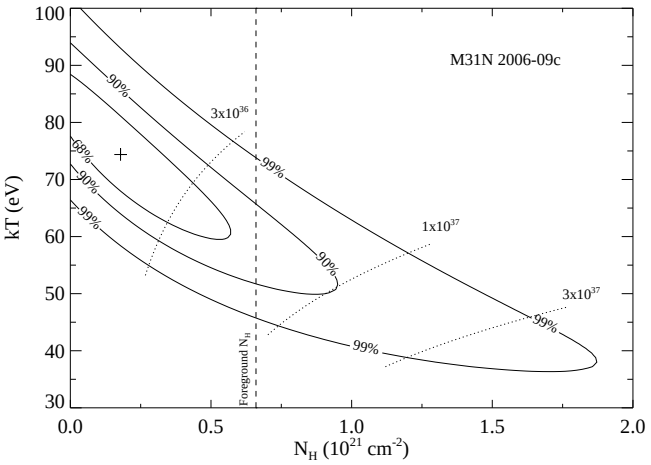

Fig. 7. Same as Fig. 3 for M31N 2006-09c in 2007/8.

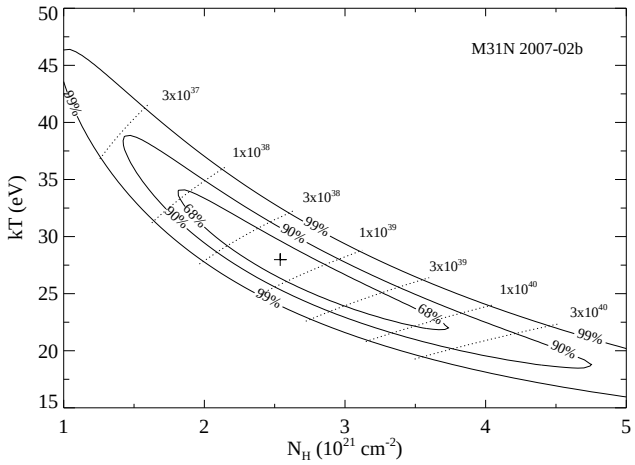

Fig. 8. Same as Fig. 3 for M31N 2007-02b in 2008/9.

counterpart was detected in the first XMM-Newton observation of 2007/8 (see Table 5). However, the preceding *Chandra* observations only provided upper limits that are larger than the XMM-Newton luminosities. Therefore, we could not determine if the source was already active on a similar level during these observations. From the upper limits given in Paper I we deduce that the source was not detectable 140 days after optical outburst with an upper limit of $L_x < 0.9 \times 10^{36}$ erg s^{-1}. The turn-on time given in Table 10 is estimated as the midpoint between day 140 and the first detection of the source given in Table 5. Similarly, due to the faintness of the source it was not clear if the non-detections in the last two XMM-Newton observations of 2007/8 correspond to the X-ray turn-off of the source. For Table 10 we therefore estimated the actual turn-off of the source to have occurred in between the last 2007/8 and the first 2008/9 observation of XMM-Newton.

The combined XMM-Newton EPIC PN spectra of the X-ray counterpart can be best fitted with an absorbed blackbody model with $kT = 74^{+20}_{-24}$ eV and $N_{\rm H} = (0.2^{+0.8}_{-0.2}) \times 10^{21}$ cm^{-2} which classifies this source as a SSS. Note, that the formal best-fitting $N_{\rm H}$ is smaller than the Galactic foreground absorption of $\sim 6.7 \times 10^{20}$ cm^{-2}. Therefore, we used the confidence contours for absorption column density and blackbody temperature of the model (see Fig. 7) to estimate an $kT = (59 \pm 7)$ eV, assuming Galactic foreground absorption.

3.2.5. M31N 2007-02b

The optical nova was discovered by K. Hornoch[7] on 2007-02-03. It was spectroscopically confirmed by Pietsch et al. (2007a) and A. Shafter[8] who classified it as hybrid nova and Fe II nova respectively. An X-ray counterpart was detected in the third XMM-Newton observation of 2007/8 (see Table 5). However, the source is right on the edge of the XMM-Newton field of view in this observation and its position is not covered in the first two 2007/8 observations due to the changing roll angle. The large distance of the nova from the M 31 centre might also be the reason for its non-detection by *Chandra* in 2007/8 and 2008/9. This is because the *Chandra* PSF strongly degrades towards high off-axis angles, an effect which decreases the detection sensitivity significantly. We therefore assume that the source was active from the third 2007/8 until at least the last 2008/9 observation of XMM-Newton. The source luminosity significantly increased from one campaign to the next (Table 5).

The XMM-Newton EPIC PN spectra of 2007/8 and 2008/9 could be fit with absorbed black body models, the parameters of which were in agreement within the errors. We therefore performed a simultaneous modelling of both spectra which resulted in best fit $kT = (28 \pm 10)$ eV and $N_{\rm H} = (2.5^{+1.8}_{-1.1}) \times 10^{21}$ cm^{-2}, allowing us to classify this source as a SSS. Confidence contours for absorption column density and blackbody temperature are shown in Fig. 8.

3.2.6. M31N 2007-10b

The optical nova was discovered by Burwitz et al. (2007) on 2007-10-13.26 UT. The start of the nova outburst was determined with the accuracy of less than a day from a non-detection on 2007-10-12.40 UT (Burwitz et al. 2007). Based on optical spectra, Rau et al. (2007) classified the object as a He/N nova. They further reported an expansion velocity of 1450 ± 100 km s^{-1} and noted that this value is atypically low for He/N novae. An X-ray counterpart was already present in the first *Chandra* observation of 2007/8. Initially, the source was bright ($L_x \sim 3 \times 10^{37}$ erg s^{-1}) but its luminosity declined fast (see Table 5). The nova exhibited a short SSS state with a duration of less than 100 days. The XMM-Newton EPIC PN spectrum therefore only contained few counts. It can be best fitted with an absorbed blackbody model with $kT = 66^{+34}_{-24}$ eV and $N_{\rm H} = (0.9^{+1.5}_{-0.8}) \times 10^{21}$ cm^{-2}, classifying this source as a SSS. Confidence contours for absorption column density and blackbody temperature are shown in Fig. 9.

3.2.7. M31N 2007-12d

The optical nova was discovered independently by Henze et al. (2007) and Nishiyama & Kabashima[9] on 2007-12-17.58 UT. The accuracy of the time of the nova outburst is about 0.4 days, based on a non-detection on 2007-12-17.19 UT (Burwitz et al. 2008; Henze et al. 2007). From our optical data obtained following the discovery by Henze et al. (2007) we estimate a very fast decline of the optical light curve ($t_2 \sim 4$ days). The object was classified as a He/N nova by Shafter (2007a), who reported strong and broad Balmer lines with a FWHM for Hα of about

[7] see http://www.cfa.harvard.edu/iau/CBAT_M31.html#2007-02b

[8] see http://mintaka.sdsu.edu/faculty/shafter/extragalactic_novae/HET/

[9] see http://www.cfa.harvard.edu/iau/CBAT_M31.html#2007-12d

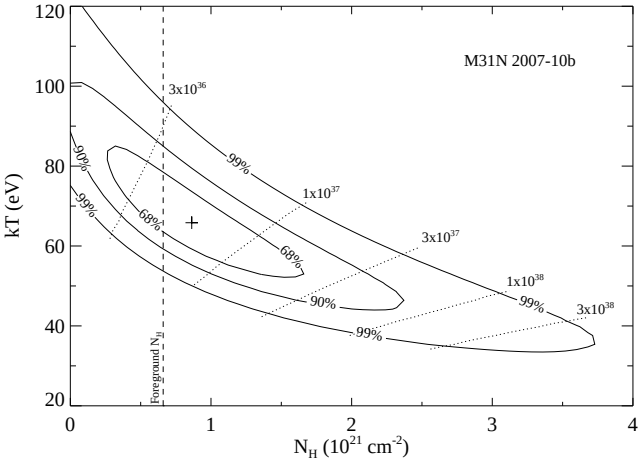

Fig. 9. Same as Fig. 3 for M31N 2007-10b in 2007/8.

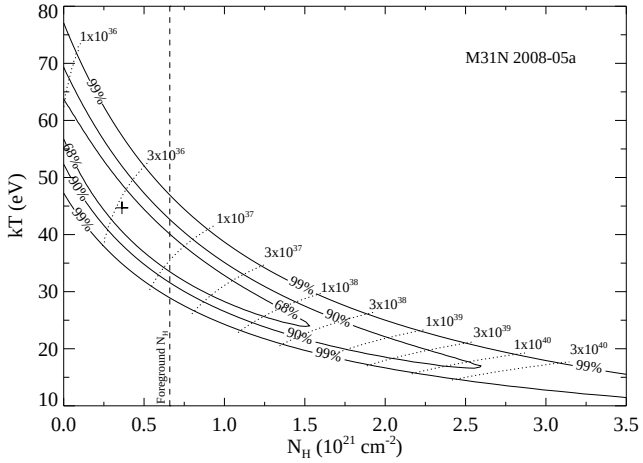

Fig. 10. Same as Fig. 3 for M31N 2008-05a in 2008/9.

5500 km s^{-1}. The line width implies a high ejection velocity of the nova envelope of about 2750 km s^{-1}. Together with the fast decline of the optical light curve this implies a rapidly evolving nova.

A faint X-ray counterpart (L_x = (2.8 ± 0.8) ×10^{36} erg s^{-1}) was visible in only one XMM-Newton observation about 22 days after outburst (see Table 5). Unfortunately, there are too few source counts to perform a spectral fit for this source. However, we can classify it as a SSS based on the hardness ratio criterion described in Sect.2.

Nothing was found at the position of M31N 2007-12d in X-ray data on day 12 and 32 after outburst with upper limits of $L_x \lesssim 1.5 \times 10^{36}$ erg s^{-1}. This indicates that the nova exhibited an extremely short SSS state of less than 20 days, supporting the interpretation of a very fast nova suggested by its optical properties. The speed of the nova evolution is remarkable, because it makes M31N 2007-12d not only the fastest SSS in our sample (see Table 10), but more so, the fastest of *all* novae known so far, for which SSS emission was found. Its SSS duration is considerably shorter than those of the M 31 novae M31N 2007-11a and M31N 2007-12b (see Table 5) as well as those of the Galactic RNe RS Oph (about 60 days, Osborne et al. 2006) and even U Sco (about 28 days Schaefer et al. 2010; Schlegel et al. 2010). For all of these nova systems it was discussed that they might contain a massive WD (Kahabka et al. 1999; Hachisu et al. 2007; Henze et al. 2009b) (Pietsch et al., in prep.). The SSS duration of nova V2491 Cyg could be of comparable length, but its turn-on time is longer (about 35 days, Page et al. 2010). In fact, so far V2491 Cyg and the two RNe mentioned above are the only Galactic novae with a short SSS phase of less than 100 days. Note, that V2491 Cyg is discussed as a candidate RN in Page et al. (2010). Implications on the possible connection of RNe with M31N 2007-12d and other fast novae in our sample are discussed in Sect. 5.4.

3.2.8. M31N 2008-05a

The optical nova was discovered by Nishiyama & Kabashima[10] on 2008-05-15 and confirmed by Henze et al. (2008c) using Hα observations. Immler et al. (2008) report *Swift* Ultraviolet/Optical Telescope (UVOT) detections of the source on 2008-05-26. An X-ray counterpart became visible in 2008/9 and its light curve, shown in Table 5, indicates significant variability by a factor of three or more. The turn-on time of the source is estimated as the midpoint between observations 9826 and 9827. The object was still detected at the end of the 2008/9 campaign, therefore we can only give a lower limit for its X-ray turn-off (see Table 10).

The XMM-Newton EPIC spectrum of the source can be best fitted by an absorbed black body model with $N_{\rm H}$ = ($0.4^{+1.8}_{-0.4}$) ×10^{21} cm^{-2} and $kT = 45^{+25}_{-28}$ eV, classifying this source as a SSS. Note, that the formal best-fit $N_{\rm H}$ is smaller than the Galactic foreground absorption of ∼ 6.7 ×10^{20} cm^{-2} (but still compatible with it within the errors). Confidence contours for absorption column density and blackbody temperature are shown in Fig. 10.

3.2.9. M31N 2008-05b

The optical nova was discovered by Nishiyama & Kabashima[11] on 2008-05-23. It was confirmed as a nova by Henze et al. (2008c), using Hα observations. Immler et al. (2008) report *Swift* UVOT detections on 2008-05-27. A faint X-ray counterpart is detected in four consecutive *Chandra* HRC-I observations 190 – 209 days after the outburst (see Table 5). The source is not detected in the two earlier *Chandra* observations, nor in the last two observations of the 2008/9 campaign. We estimate the turn-on (turn-off) time as the midpoint between observations 9826 and 9827 (10838 and 0551690201). There is no significant variability during the duration of the X-ray visibility.

3.2.10. M31N 2008-06a

The optical nova was discovered by Henze et al. (2008a) on 2008-06-14. An optical re-brightening of the object was observed on 2008-09-01 by Valcheva et al. (2008) (see also Ovcharov et al. 2009). Henze et al. (2008c) confirmed the object as a nova on the basis of Hα observations. A faint X-ray counterpart only appeared after 257 days in the very last observation of the 2008/9 campaign (see Table 5).

[10] see http://www.cfa.harvard.edu/iau/CBAT_M31.html#2008-05a

[11] see http://www.cfa.harvard.edu/iau/CBAT_M31.html#2008-05b

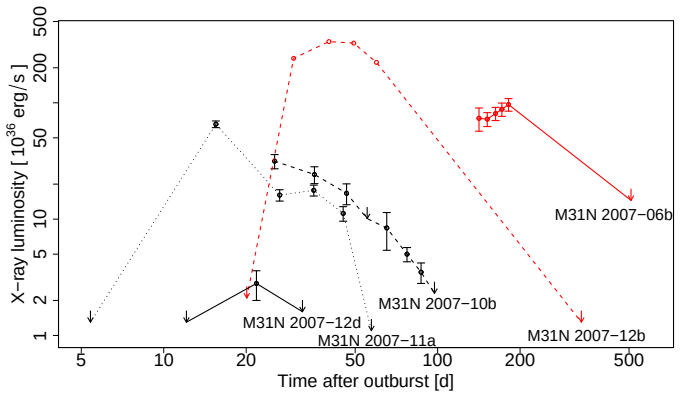

Fig. 11. X-ray light curves for all novae detected in 2007/8 and 2008/9 with short (< 100 days) SSS turn-on times. Note the logarithmic axes. Detections are indicated as open circles with error bars and upper limits as down-pointing arrows. For nova M31N 2007-12b the error bars are smaller than the size of the symbols. Measurements for each nova are connected by lines, the style and colour of which differentiates between the novae.

3.3. Upper limits for non-detected X-ray emission of optical novae

The two novae M31N 2001-01a and M31N 2005-02a were active SSSs until the end of the observations reported in Paper I. These sources are not detected anymore (see Table 6). Upper limits for undetected novae with optical outburst from October 2006 till February 2008 and October 2007 till February 2009 are listed in Tables 7 and 8 for the 2007/8 and 2008/9 campaigns, respectively. We assume that nova M31N 2006-12d, which was reported by K. Hornoch[12], was actually caused by a re-brightening of nova M31 2006-11b because the positions of both novae are nearly identical.

3.4. Non-nova supersoft sources

Additionally, we searched our XMM-Newton data for SSSs which do not have nova counterparts. This search was based on the hardness-ratio criterion described in Eq. 1 in Sect. 2. As a result, we found three sources which are already known SSSs. The light curves of these objects, all of which were also detected in Paper I, are given in Table 9 and their positions are shown in Fig. 1. In the following, we describe briefly the properties of these sources in our observations. We refer to the objects by their names in the catalogue of time-variable X-ray source by Stiele et al. (2008), which contains all three sources.

Object XMMM31 J004252.5+411541 is a bright and persistent SSS (see Table 9) that has already been discovered with the *Einstein Observatory* (source 69 in Trinchieri & Fabbiano 1991). It was extensively discussed by Trudolyubov & Priedhorsky (2008), who reported X-ray pulsations with a period of about 217.7 s. They discussed the source as a magnetic WD that is steadily accreting and burning material. During our monitoring, the source was always detected with high luminosities ($L_x > 10^{38}$ erg s^{-1}). Its light curve was variable by a factor of about two at most (see Table 9).

Object XMMM31 J004318.8+412017 was already discovered in early *Chandra* observations (Kaaret 2002; Kong et al. 2002). Williams et al. (2006) included it in their catalogue of transient X-ray sources in M 31 (named r3-8 there, from its designation in Kong et al. 2002) and discussed it as a Galactic foreground polar based on its soft spectrum. During our monitoring the source showed burst-like variability with luminosity increase by more than a factor of ten (see Table 9). This behaviour agrees with Williams et al. (2006) who also reported four outbursts of the source.

Object XMMM31 J004318.7+411804 was reported as a previously unknown variable SSS by Stiele et al. (2008). They reported a maximum luminosity of $L_x = 3.3{\times}10^{36}$ erg s^{-1} and classified the source as a candidate SSS. The object is detected in less than half of our monitoring observations (see Table 9). Its luminosity is only a few 10^{36} erg s^{-1} in most detections with the exception of two *Chandra* observations were it reaches $\sim 10^{37}$ erg s^{-1}.

To summarise, in the two monitoring campaigns we found in total 17 X-ray nova counterparts. Thirteen of these sources have been classified as SSSs. Comparing this number to the three non-nova SSSs presented here, we can again confirm the finding of PFF2005 that optical novae are the major class of SSSs in the central part of M 31.

4. Novae with X-ray counterpart in M 31 - the catalogue

We compiled a catalogue of optical novae with an X-ray counterpart in M 31. This catalogue contains 60 objects and is mainly based ($\sim$ 85%) on the results of our monitoring campaigns for M 31 novae (presented here and in Paper I) and on our analysis of archival M 31 X-ray data (in PFF2005 and PHS2007). We searched the available literature and included further X-ray detections and measurements of M 31 novae reported by the following authors: Smirnova et al. (2006), Pietsch et al. (2007c), Voss et al. (2008), Orio & Nelson (2008), Nelson et al. (2008a), and Stiele et al. (2010). To our knowledge, the catalogue contains all known M 31 novae with an X-ray counterpart discovered until the end of February 2009.

We did not include five apparent X-ray nova counterparts from a recent census of SSSs in M 31 (Orio et al. 2010), because we cannot confirm them in our data. These sources are the suggested X-ray counterparts of the novae M31N 2004-09b, M31N 2007-08b, M31N 2007-11c, M31N 2008-02a and M31N 2008-06c (table 3 in Orio et al. 2010). In the cases of M31N 2007-11c and M31N 2008-06c the positions of the optical novae are relatively close to known non-SSS X-ray sources in the field (sources 388 and 405 from Pietsch et al. 2005b, respectively), which might have been mis-identified as nova counterparts.

Our catalogue is presented in Table 10 and contains the following information: (a) for the optical nova: the name, date of outburst detection, maximum observed magnitude in a certain filter (which is not necessarily the peak magnitude of the nova), t_2 decay time in the R band, spectroscopic nova type in the classification scheme of Williams (1992), and expansion velocity of the ejected envelope as measured from the earliest optical spectrum (half of the FWHM of the Hα line); (b) for the X-ray counterpart: the turn-on and turn-off times, a flag for SSS classification, the X-ray luminosity, and the blackbody temperature as inferred from the X-ray spectrum; (c) derived parameters: the ejected and burned masses as computed according to Sect. 5.3; (d) references. Note, that not all parameter values are known for all objects. The full catalogue will be available in electronic form at the CDS.

[12] see http://www.cfa.harvard.edu/iau/CBAT_M31.html#2007-12d

Table 5. M 31 optical novae with XMM-Newton and *Chandra* counterparts discovered in this work.

Optical nova candidate			X-ray measurements				
Name M31N	RA (h:m:s)[a] Dec (d:m:s)[a]	MJD[b] (d)	D[c] ($''$)	Observation[d] ID	Δt[e] (d)	L_X^f (10^{36} erg s^{-1})	Comment[g]
2003-08c	0:42:41.2	52878.0		8526 (HRC-I)	1533.6	< 2.1	
	41:16:16.0		0.4	8527 (HRC-I)	1543.8	3.5 ± 0.7	
				8528 (HRC-I)	1554.8	< 3.3	
				8529 (HRC-I)	1563.6	2.6 ± 0.8	
			0.3	8530 (HRC-I)	1573.5	3.6 ± 0.8	
				mrg1 (EPIC)	1585.6	< 11.3	
				9825 (HRC-I)	1900.3	< 0.8	
			0.5	9826 (HRC-I)	1909.1	5.3 ± 1.1	
			0.3	9827 (HRC-I)	1920.2	4.7 ± 1.0	
			0.3	9828 (HRC-I)	1929.4	5.5 ± 1.1	
				9829 (HRC-I)	1940.0	< 6.2	
				10838 (HRC-I)	1940.5	< 5.0	
				mrg2 (EPIC)	1952.1	< 7.0	
				10683 (HRC-I)	2000.9	< 3.2	
			0.2	10684 (HRC-I)	2010.2	2.7 ± 0.8	
2004-01b	0:42:41.19	53005.8		8530 (HRC-I)	1445.7	< 1.6	
	41:15:45.0		0.4	9825 (HRC-I)	1772.6	5.0 ± 1.1	
			0.2	9826 (HRC-I)	1781.4	5.9 ± 1.2	
			0.4	9827 (HRC-I)	1792.5	5.1 ± 1.1	
			0.3	9828 (HRC-I)	1801.7	5.8 ± 1.3	
			0.4	9829 (HRC-I)	1812.3	5.7 ± 1.3	
			0.2	10838 (HRC-I)	1812.7	7.1 ± 1.5	
				mrg2 (EPIC)	1824.4	< 22.3	
			0.1	10683 (HRC-I)	1873.1	11.1 ± 1.6	
			0.1	10684 (HRC-I)	1882.4	8.7 ± 1.7	
2006-06b	0:42:32.77	53869.0		0505720601 (EPIC)	634.2	< 1.8	SSS
	41:16:49.2		0.4	9825 (HRC-I)	909.3	3.3 ± 0.7	
				9826 (HRC-I)	918.1	< 2.6	
			0.5	9827 (HRC-I)	929.2	1.9 ± 0.6	
			0.3	9828 (HRC-I)	938.4	2.8 ± 0.6	
			0.1	9829 (HRC-I)	949.0	3.3 ± 1.2	
				10838 (HRC-I)	949.5	< 3.3	
			0.9	0551690201 (EPIC)	961.1	3.3 ± 0.5	
			0.3	0551690301 (EPIC)	971.3	2.9 ± 0.5	
				0551690401 (EPIC)	977.9	< 5.8	
			0.3	0551690501 (EPIC)	989.3	4.4 ± 0.6	
			0.8	0551690601 (EPIC)	997.6	4.0 ± 0.9	
			0.1	10683 (HRC-I)	1009.9	10.9 ± 1.7	
			0.2	10684 (HRC-I)	1019.2	7.2 ± 1.4	
2006-09c	0:42:42.38	53996.2		mrg1 (HRC-I)	415.4	< 4.3	SSS
	41:08:45.5		1.2	0505720201 (EPIC)	467.3	2.5 ± 0.6	
			0.5	0505720301 (EPIC)	477.0	1.6 ± 0.6	
			1.0	0505720401 (EPIC)	487.4	2.8 ± 0.8	
				0505720501 (EPIC)	496.7	< 2.7	
				0505720601 (EPIC)	507.0	< 1.9	
				mrg2 (EPIC)	833.9	< 0.3	
2007-02b	0:41:40.32	54134.8	1.0	0505720401 (EPIC)	348.9	1.8 ± 0.7	SSS
	41:14:33.5			0505720501 (EPIC)	358.2	< 5.6	
			0.5	0505720601 (EPIC)	368.5	6.2 ± 1.1	
			0.7	0551690201 (EPIC)	695.4	17.4 ± 5.3	
			1.3	0551690301 (EPIC)	705.5	17.5 ± 5.4	
			3.0	0551690401 (EPIC)	712.1	9.7 ± 3.0	
			0.2	0551690501 (EPIC)	723.6	9.7 ± 1.2	
			1.2	0551690601 (EPIC)	731.8	10.5 ± 1.8	

Table 5. continued.

Optical nova candidate			X-ray measurements				
Name M31N	RA (h:m:s)[a] Dec (d:m:s)[a]	MJD[b] (d)	D[c] ($''$)	Observation[d] ID	Δt[e] (d)	$L_{\rm X}^{f}$ (10^{36} erg s^{-1})	Comment[g]
2007-06b	0:42:33.14	54270.0	9.4	8526 (HRC-I)	141.6	73.6 ± 16.6	SSS
	41:00:25.9		1.2	8527 (HRC-I)	151.8	72.4 ± 9.9	see (1)
			9.7	8528 (HRC-I)	162.8	80.9 ± 10.5	
			0.6	8529 (HRC-I)	171.6	88.0 ± 11.5	
			5.9	8530 (HRC-I)	181.5	96.7 ± 12.0	
				mrg2 (HRC-I)	508.3	< 14.5	
2007-10b	0:43:29.48	54386.2	1.2	8526 (HRC-I)	25.4	31.5 ± 4.4	SSS
	41:17:13.5		2.4	8527 (HRC-I)	35.5	24.2 ± 4.0	
			2.5	8528 (HRC-I)	46.5	16.7 ± 3.4	
				8529 (HRC-I)	55.3	< 10.1	
				8530 (HRC-I)	65.2	8.4 ± 3.0	
			1.8	0505720201 (EPIC)	77.3	5.0 ± 0.7	
			1.0	0505720301 (EPIC)	87.0	3.5 ± 0.7	
				0505720401 (EPIC)	97.4	< 2.3	
				0505720501 (EPIC)	106.7	< 2.1	
				0505720601 (EPIC)	117.0	< 0.6	
2007-11a	0:42:37.29	54406.2		8526 (HRC-I)	5.4	< 1.3	SSS-HR
	41:17:10.3		0.4	8527 (HRC-I)	15.5	65.5 ± 4.3	
			0.3	8528 (HRC-I)	26.5	16.1 ± 1.8	see (2)
			0.2	8529 (HRC-I)	35.3	17.7 ± 1.9	
			0.2	8530 (HRC-I)	45.2	11.2 ± 1.6	
				0505720201 (EPIC)	57.3	< 1.1	
				0505720301 (EPIC)	67.0	< 2.3	
				0505720401 (EPIC)	77.4	< 2.6	
				0505720501 (EPIC)	86.7	< 1.9	
				0505720601 (EPIC)	97.0	< 3.2	
2007-12b	0:43:19.94	54443.5		8530 (HRC-I)	8.0	< 3.5	SSS
	41:13:46.6			0505720201 (EPIC)	20.1	< 2.1	see (3)
			0.8	0505720301 (EPIC)	29.8	241.1 ± 3.1	
			0.8	0505720401 (EPIC)	40.1	335.8 ± 3.8	
			0.7	0505720501 (EPIC)	49.4	326.0 ± 5.2	
			0.6	0505720601 (EPIC)	59.8	222.5 ± 3.8	
				mrg2 (HRC-I)	334.8	< 1.3	
				mrg2 (EPIC)	386.6	< 0.2	
2007-12d	0:41:54.96	54451.5		0505720201 (EPIC)	12.1	< 1.3	SSS-HR
	41:09:47.3		0.9	0505720301 (EPIC)	21.8	2.8 ± 0.8	
				0505720401 (EPIC)	32.1	< 1.6	
				0505720501 (EPIC)	41.4	< 0.5	
				0505720601 (EPIC)	51.8	< 1.3	
2008-05a	0:42:56.84	54600.8		9825 (HRC-I)	177.6	< 4.4	SSS
	41:11:52.4			9826 (HRC-I)	186.4	< 4.9	
			0.4	9827 (HRC-I)	197.5	7.3 ± 1.8	
				9828 (HRC-I)	206.7	3.5 ± 1.5	
				9829 (HRC-I)	217.3	< 5.7	
				10838 (HRC-I)	217.7	5.8 ± 2.5	
				0551690201 (EPIC)	229.4	< 1.9	
				0551690301 (EPIC)	239.5	< 3.3	
				0551690401 (EPIC)	246.1	< 4.2	
			0.6	0551690501 (EPIC)	257.6	3.5 ± 0.6	
			1.1	0551690601 (EPIC)	265.8	8.3 ± 1.3	
			0.4	10683 (HRC-I)	278.1	11.1 ± 1.9	
				10684 (HRC-I)	287.4	5.3 ± 1.8	

Table 5. continued.

Optical nova candidate			X-ray measurements				
Name M31N	RA (h:m:s)[a] Dec (d:m:s)[a]	MJD[b] (d)	D^c ($''$)	Observation[d] ID	Δt^e (d)	L_X^f (10^{36} erg s^{-1})	Comment[g]
2008-05b	0:42:52.88	54608.8		9825 (HRC-I)	169.6	< 5.1	
	41:16:39.4			9826 (HRC-I)	178.4	< 5.5	
			1.4	9827 (HRC-I)	189.5	3.5 ± 0.9	
			1.0	9828 (HRC-I)	198.7	4.9 ± 1.3	
				mrg3 (HRC-I)	209.3	3.6 ± 1.1	
				mrg2 (EPIC)	221.4	< 3.2	
				10683 (HRC-I)	270.1	< 1.7	
				10684 (HRC-I)	279.4	< 2.3	
2008-06a	0:42:37.72	54631.5		9825 (HRC-I)	146.8	< 1.1	
	41:12:30.0			9826 (HRC-I)	155.6	< 2.7	
				9827 (HRC-I)	166.7	< 1.0	
				9828 (HRC-I)	175.9	< 2.2	
				9829 (HRC-I)	186.5	< 1.9	
				10838 (HRC-I)	187.0	< 2.8	
				0551690201 (EPIC)	198.6	< 0.2	
				0551690301 (EPIC)	208.8	< 3.3	
				0551690401 (EPIC)	215.4	< 1.6	
				0551690501 (EPIC)	226.8	< 1.6	
				0551690601 (EPIC)	235.1	< 2.3	
				10683 (HRC-I)	247.4	< 4.9	
			0.7	10684 (HRC-I)	256.7	3.2 ± 1.3	

Notes: As for Table 4. Additional comments refer to individual sources discussed in detail in the following papers: (1): Henze et al. (2009a), (2): Henze et al. (2009b), (3): Pietsch et al. (2010, in prep.)

Table 6. Upper limits for non-detected M 31 CNe from Paper I.

Optical nova candidate			X-ray measurements			
Name M31N	RA (h:m:s)[a] Dec (d:m:s)[a]	MJD[b] (d)	Observation[d] ID	Δt^e (d)	L_X^f (10^{36} erg s^{-1})	Comment
2001-01a	0:42:21.49	51928.8	mrg1 (HRC-I)	2482.9	< 1.5	very faint
	41:07:47.4		mrg1 (EPIC)	2534.8	< 0.6	in Paper I
2005-02a	0:42:52.79	53419.8	mrg1 (HRC-I)	991.9	< 0.5	
	41:14:28.9		mrg1 (EPIC)	1043.8	< 1.8	

Notes: As for Table 4.

Table 7. Upper limits for M 31 CN with outburst from about one year before the start of the 2007/8 monitoring till its end.

Optical nova candidate		X-ray measurements				
Name M31N	RA (h:m:s)[a] Dec (d:m:s)[a]	MJD[b] (d)	Observation[d] ID	Δt[e] (d)	L_X^f (10^{36} erg s^{-1})	Comment[g]
2006-10a	0:41:43.23	54030.8	mrg1 (HRC-I)	380.9	< 6.2	
	41:11:45.9		mrg1 (EPIC)	432.8	< 2.6	
2006-11b	0:42:44.05	54058.0	mrg1 (HRC-I)	353.6	< 0.4	later re-brightening
	41:15:02.2		mrg1 (EPIC)	405.6	< 7.3	as M31N 2006-12d
2006-11a	0:42:56.81	54063.8	mrg1 (HRC-I)	347.9	< 2.8	
	41:06:18.4		mrg1 (EPIC)	399.8	< 0.1	
2006-11c	0:41:33.23	54069.8	mrg1 (HRC-I)	341.9	< 11.3	far off-axis
	41:10:12.3					not in EPIC field of view
2006-12a	0:42:21.09	54085.0	mrg1 (HRC-I)	326.6	< 0.9	
	41:13:45.3		mrg1 (EPIC)	378.6	< 0.9	
2006-12b	0:42:11.14	54092.8	mrg1 (HRC-I)	318.9	< 6.4	
	41:07:43.8		mrg1 (EPIC)	370.8	< 0.1	
2006-12c	0:42:43.27	54093.8	mrg1 (HRC-I)	317.9	< 0.6	
	41:17:48.1		mrg1 (EPIC)	369.8	< 0.5	
2007-01a	0:42:51.13	54114.8	mrg1 (HRC-I)	296.9	< 0.8	
	41:14:33.1		mrg1 (EPIC)	348.8	< 1.8	
2007-02c	0:42:39.96	54140.8	mrg1 (HRC-I)	270.9	< 0.2	
	41:17:21.9		mrg1 (EPIC)	322.8	< 1.4	
2007-03a	0:42:53.60	54163.8	mrg1 (HRC-I)	247.9	< 2.5	
	41:12:09.8		mrg1 (EPIC)	299.8	< 2.5	
2007-05a	0:43:02.61	54238.0	mrg1 (HRC-I)	173.6	< 0.5	
	41:14:41.4		mrg1 (EPIC)	225.6	< 0.8	
2007-06a	0:41:58.40	54265.0	mrg1 (HRC-I)	146.6	< 0.8	
	41:14:10.9		mrg1 (EPIC)	198.6	< 0.1	
2007-07a	0:43:04.05	54286.0	mrg1 (HRC-I)	125.6	< 0.3	
	41:17:08.3		mrg1 (EPIC)	177.6	< 0.2	
2007-07b	0:42:45.89	54289.0	mrg1 (HRC-I)	122.6	< 0.5	
	41:18:04.2		mrg1 (EPIC)	174.6	< 0.4	
2007-07c	0:43:03.29	54300.0	mrg1 (HRC-I)	111.6	< 0.3	
	41:14:52.9		mrg1 (EPIC)	163.6	< 1.2	
2007-07d	0:42:59.49	54305.0	mrg1 (HRC-I)	106.6	< 0.5	
	41:15:06.5		mrg1 (EPIC)	158.6	< 1.3	
2007-07e	0:42:43.29	54306.5	mrg1 (HRC-I)	105.1	< 1.0	
	41:17:44.1		mrg1 (EPIC)	157.1	< 0.9	
2007-08e	0:42:44.70	54333.0	mrg1 (HRC-I)	78.6	< 0.8	
	41:16:36.2		mrg1 (EPIC)	130.6	< 28.8	close to M 31 centre
2007-08c	0:42:29.40	54342.0	mrg1 (HRC-I)	69.6	< 0.8	
	41:18:24.8		mrg1 (EPIC)	121.6	< 0.4	
2007-10a	0:42:55.95	54379.0	mrg1 (HRC-I)	32.6	< 9.9	far off-axis
	41:03:22.0					not in EPIC field of view
2007-11c	0:43:04.14	54416.0	8527 (HRC-I)	5.8	< 3.8	
	41:15:54.3		8528 (HRC-I)	16.8	< 2.0	
			8529 (HRC-I)	25.6	< 3.1	
			8530 (HRC-I)	35.5	< 3.8	
			505720 (EPIC)	47.6	< 1.9	
2008-01a	0:42:58.54	54485.2	505720501 (EPIC)	7.7	< 2.2	
	41:14:44.1		505720601 (EPIC)	18.0	< 1.4	

Notes: As for Table 4.

Table 8. Upper limits for M 31 CN with outburst from about one year before the start of the 2008/9 monitoring till its end.

Optical nova candidate			X-ray measurements			
Name M31N	RA (h:m:s)[a] Dec (d:m:s)[a]	MJD[b] (d)	Observation[d] ID	Δt[e] (d)	L_X^f (10^{36} erg s^{-1})	Comment[g]
2007-10a	0:42:55.95 41:03:22.0	54379.0	mrg2 (HRC-I)	399.3	< 17.0	far off-axis not in EPIC field of view
2007-11c	0:43:04.14 41:15:54.3	54416.0	mrg2 (HRC-I)	362.3	< 0.5	
			mrg2 (EPIC)	414.1	< 2.3	
2008-01a	0:42:58.54 41:14:44.1	54485.2	mrg2 (HRC-I)	293.1	< 0.6	
			mrg2 (EPIC)	344.9	< 0.6	
2008-02a	0:42:30.38 41:09:53.8	54503.2	mrg2 (HRC-I)	275.1	< 0.9	
			mrg2 (EPIC)	326.9	< 1.0	
2008-03b	0:42:34.21 41:16:44.4	54527.8	mrg2 (HRC-I)	250.6	< 0.6	
			mrg2 (EPIC)	302.4	< 1.3	
2008-05c	0:43:12.08 41:19:15.8	54612.5	mrg2 (HRC-I)	165.8	< 2.2	
			mrg2 (EPIC)	217.6	< 0.4	
2008-07a	0:42:34.42 41:18:15.7	54619.0	mrg2 (HRC-I)	159.3	< 0.6	
			mrg2 (EPIC)	211.1	< 0.1	
2008-06b	0:42:27.81 41:14:48.2	54643.0	mrg2 (HRC-I)	135.3	< 0.8	
			mrg2 (EPIC)	187.1	< 0.4	
2008-06c	0:43:08.30 41:18:38.0	54645.0	mrg2 (HRC-I)	133.3	< 1.7	
			mrg2 (EPIC)	185.1	< 0.3	
2008-07b	0:43:27.28 41:10:03.3	54669.2	mrg2 (HRC-I)	109.1	< 4.0	
			mrg2 (EPIC)	160.9	< 0.6	
2008-08a	0:42:44.99 41:17:07.7	54688.0	mrg2 (HRC-I)	90.3	< 1.7	
			mrg2 (EPIC)	142.1	< 3.0	
2008-08b	0:42:52.38 41:16:12.9	54688.0	mrg2 (HRC-I)	90.3	< 1.5	
			mrg2 (EPIC)	142.1	< 5.4	
2008-08c	0:42:40.51 41:26:18.0	54706.2	mrg2 (HRC-I)	72.1	< 1.8	
			mrg2 (EPIC)	123.9	< 0.3	
2008-09a	0:41:46.72 41:07:52.1	54722.2	mrg2 (HRC-I)	56.1	< 13.5	far off-axis
			mrg2 (EPIC)	107.9	< 0.9	
2008-09c	0:42:51.42 41:01:54.0	54724.2	mrg2 (HRC-I)	54.1	< 18.1	far off-axis not in EPIC field of view
2008-10b	0:43:02.42 41:14:09.9	54745.0	mrg2 (HRC-I)	33.3	< 2.5	
			mrg2 (EPIC)	85.1	< 0.6	
2008-10c	0:42:48.50 41:13:49.8	54759.0	mrg2 (HRC-I)	19.3	< 0.8	
			mrg2 (EPIC)	71.1	< 0.1	
2008-11d	0:42:57.30 41:15:41.1	54795.0	9827 (HRC-I)	3.2	< 1.1	
			9828 (HRC-I)	12.4	< 1.2	
			9829 (HRC-I)	23.0	< 1.2	
			10838 (HRC-I)	23.5	< 1.3	
			mrg2 (EPIC)	35.1	< 1.1	
			10683 (HRC-I)	83.9	< 2.7	
			10684 (HRC-I)	93.2	< 2.1	
2008-12b	0:43:04.85 41:17:51.6	54829.8	551690201 (EPIC)	0.4	< 1.9	
			551690301 (EPIC)	10.5	< 3.0	
			551690401 (EPIC)	17.1	< 4.8	
			551690501 (EPIC)	28.6	< 6.3	
			551690601 (EPIC)	36.8	< 3.4	
			10683 (HRC-I)	49.1	< 0.6	
			10684 (HRC-I)	58.4	< 0.6	
2009-02b	0:42:27.77 41:13:42.4	54882.2	10684 (HRC-I)	5.9	< 1.9	

Notes: As for Table 4.

Table 9. Non-nova SSSs detected during the monitoring.

Name[a] XMMM31	RA (h:m:s)[b] Dec (d:m:s)[a]	Observation ID	MJD[c] (d)	L_X^d (10^{36} erg s^{-1})	Comment[e]
J004252.5+411541	00:42:52.50 41:15:40.1	8526 (HRC-I)	54411.6	267.1 ± 9.6	217.7 s period (1)
		8527 (HRC-I)	54421.8	294.4 ± 10.2	
		8528 (HRC-I)	54432.8	361.7 ± 14.1	
		8529 (HRC-I)	54441.6	217.8 ± 11.3	
		8530 (HRC-I)	54451.5	248.7 ± 11.6	
		505720201 (EPIC)	54463.6	203.1 ± 2.3	
		505720301 (EPIC)	54473.3	228.1 ± 2.5	
		505720401 (EPIC)	54483.6	178.1 ± 2.6	
		505720501 (EPIC)	54492.9	215.7 ± 3.5	
		505720601 (EPIC)	54503.2	247.8 ± 3.1	
		9825 (HRC-I)	54778.3	156.1 ± 7.3	
		9826 (HRC-I)	54787.1	232.3 ± 9.0	
		9827 (HRC-I)	54798.2	362.2 ± 14.2	
		9828 (HRC-I)	54807.4	301.6 ± 12.8	
		9829 (HRC-I)	54818.0	261.5 ± 16.7	
		10838 (HRC-I)	54818.5	303.5 ± 18.0	
		551690201 (EPIC)	54830.1	244.5 ± 3.0	
		551690301 (EPIC)	54840.3	189.7 ± 2.6	
		551690401 (EPIC)	54846.9	224.2 ± 4.6	
		551690501 (EPIC)	54858.3	230.6 ± 3.1	
		551690601 (EPIC)	54866.6	176.0 ± 3.2	
		10683 (HRC-I)	54878.9	255.7 ± 10.8	
		10684 (HRC-I)	54888.2	224.2 ± 10.0	
J004318.8+412017	00:43:18.80 41:20:16.1	8526 (HRC-I)	54411.6	< 5.9	foreground polar(?) (2)
		8527 (HRC-I)	54421.8	< 11.0	
		8528 (HRC-I)	54432.8	< 1.6	
		8529 (HRC-I)	54441.6	< 1.5	
		8530 (HRC-I)	54451.5	10.2 ± 2.6	
		505720201 (EPIC)	54463.6	9.4 ± 0.9	
		505720301 (EPIC)	54473.3	4.6 ± 0.6	
		505720401 (EPIC)	54483.6	< 3.8	
		505720501 (EPIC)	54492.9	5.3 ± 0.9	
		505720601 (EPIC)	54503.2	1.1 ± 0.4	
		9825 (HRC-I)	54778.3	20.5 ± 5.4	
		9826 (HRC-I)	54787.1	14.5 ± 4.2	
		9827 (HRC-I)	54798.2	< 2.7	
		9828 (HRC-I)	54807.4	< 1.6	
		9829 (HRC-I)	54818.0	< 7.2	
		10838 (HRC-I)	54818.5	< 10.8	
		551690201 (EPIC)	54830.1	3.0 ± 0.6	
		551690301 (EPIC)	54840.3	2.5 ± 0.7	
		551690401 (EPIC)	54846.9	< 3.3	
		551690501 (EPIC)	54858.3	< 1.9	
		551690601 (EPIC)	54866.6	< 2.4	
		10683 (HRC-I)	54878.9	< 7.7	
		10684 (HRC-I)	54888.2	< 3.5	

Table 9. continued.

Name[a] XMMM31	RA (h:m:s)[b] Dec (d:m:s)[a]	Observation ID	MJD[c] (d)	L_X^d (10^{36} erg s^{-1})	Comment[e]
J004318.7+411804	00:43:18.70	8526 (HRC-I)	54411.6	< 6.5	strongly variable (2)
	41:18:05.2	8527 (HRC-I)	54421.8	< 3.3	
		8528 (HRC-I)	54432.8	< 9.0	
		8529 (HRC-I)	54441.6	< 8.6	
		8530 (HRC-I)	54451.5	< 6.1	
		505720201 (EPIC)	54463.6	1.1 ± 0.4	
		505720301 (EPIC)	54473.3	0.9 ± 0.3	
		505720401 (EPIC)	54483.6	0.6 ± 0.3	
		505720501 (EPIC)	54492.9	< 6.9	
		505720601 (EPIC)	54503.2	1.7 ± 0.5	
		9825 (HRC-I)	54778.3	9.7 ± 3.3	
		9826 (HRC-I)	54787.1	< 8.1	
		9827 (HRC-I)	54798.2	< 4.3	
		9828 (HRC-I)	54807.4	< 4.3	
		9829 (HRC-I)	54818.0	< 10.1	
		10838 (HRC-I)	54818.5	9.5 ± 3.3	
		551690201 (EPIC)	54830.1	2.4 ± 0.6	
		551690301 (EPIC)	54840.3	1.9 ± 0.5	
		551690401 (EPIC)	54846.9	< 3.2	
		551690501 (EPIC)	54858.3	4.8 ± 1.9	
		551690601 (EPIC)	54866.6	< 2.1	
		10683 (HRC-I)	54878.9	< 7.2	
		10684 (HRC-I)	54888.2	< 2.8	

Notes: [a]: Source name from the catalogue of Stiele et al. (2008); [b]: RA, Dec are given in J2000.0; [c]: Modified Julian Date MJD = JD - 2 400 000.5; [d]: unabsorbed luminosity in 0.2–10.0 keV band assuming a 50 eV blackbody spectrum with Galactic foreground absorption, luminosity errors are 1σ, upper limits are 3σ; [e]: (1): Trudolyubov & Priedhorsky (2008), (2): Williams et al. (2006), (3): Orio (2006);

Table 10. Catalogue of X-ray detected optical novae in M 31.

Optical measurements						X-ray measurements						Derived parameters		References
Name M31N	Outburst[a] (JD)	Brightness[b] (mag Filter)	t_{2R} [c] (d)	Old/[d] Young	Type[e]	v_{exp} [f] (km s^{-1})	Turn on (d)	Turn off (d)	SSS?[g]	L_X^h (10^{36} erg s^{-1})	kT_{BB}^i (eV)	Ejected mass (10^{-5} $M_\odot$)	Burned mass (10^{-6} $M_\odot$)	o(ptical)[j] and x(-ray)[k]
1982-09b	2445225.01	16.7(Hα)		O		278	2874	> 4317		8.7 ± 2.4		13.18	> 7.21	o1;x1
1990-09a	2448151.94	15.7(Hα)		Y		1031	156 ± 156	501 ± 188		12.1 ± 1.9		$0.96^{+4.07}_{-0.96}$	0.84 ± 0.31	o2,3;x4,1
1990-09g	2448161.50	18.4(Hα)		O		1043	152 ± 152	842 ± 538		63.0 ± 4.0		$0.94^{+3.96}_{-0.94}$	1.41 ± 0.9	o3;x1
1990-12a	2448235.50	16.0(Hα)		O		662	417 ± 188	955 ± 188		43.0 ± 5.3		$2.32^{+7.43}_{-1.82}$	1.6 ± 0.31	o3;x1,5
1991-01b	2448280.50	16.4(Hα)		Y		696	373 ± 188	810 ± 100		88.0 ± 10.0		$2.1^{+6.94}_{-1.68}$	1.35 ± 0.17	o3;x1
1992-11b	2448935.58	16.4(Hα)		O	Fe II	790	282 ± 282	763 ± 186		13.1 ± 4.0		$1.63^{+7.46}_{-1.63}$	1.27 ± 0.31	o3;x1
1994-09a	2449622.50	17.6(R)		O		294	2529 ± 62	3121 ± 463		1.6 ± 0.2		$11.75^{+30.02}_{-8.43}$	5.21 ± 0.77	o4;x1
1995-09b	2449963.50	15.6(Hα)		O		356	1653 ± 81	3656 ± 273		16.1 ± 3.6		$8.01^{+19.94}_{-5.7}$	6.11 ± 0.46	o5;x1
1995-11c	2450048.34	16.3(Hα)		O		505	762 ± 725	3609 ± 236		13.8 ± 3.3		$3.99^{+19.98}_{-3.88}$	6.03 ± 0.39	o3,6;x1
1996-08b	2450307.50	16.1(Hα)		O		340	1831 ± 49	> 4560	spec	2.0 ± 0.3	$21.0^{+8.0}_{-13.0}$	$8.79^{+21.52}_{-6.23}$	> 7.62	o3;x1
1997-06c	2450617.50	15.6(Hα)		O		580	559 ± 559	1244 ± 326		10.6 ± 3.2		$3.02^{+15.0}_{-3.02}$	2.08 ± 0.54	o3,5;x1
1997-08b	2450661.50	16.5(Hα)		Y		366	1556 ± 34	2052 ± 463		0.7 ± 0.2		$7.59^{+18.04}_{-5.33}$	3.43 ± 0.77	o3,5;x1
1997-09a	2450718.50	16.6(B)	10.0	Y						9.6 ± 2.9				o7;x1
1997-10c	2450723.51	16.6(B)	7.9	O		447	997	1090 ± 93	spec	59.0	$41.0^{+27.0}_{-21.0}$	5.08	1.82 ± 0.16	o7;x6
1997-11a	2450753.55	18.0(R)		O		325	2027 ± 566	> 4025		4.4 ± 0.7		$9.63^{+32.17}_{-7.44}$	> 6.72	o3;x2
1998-06a	2450970.50	16.2(Hα)		O		441	1028 ± 92	1773 ± 463		1.7 ± 0.3		$5.23^{+12.83}_{-3.7}$	2.96 ± 0.77	o5;x1
1998-07d	2451019.50	15.9(Hα)		O		451	979 ± 92	1345 ± 74		80.0 ± 15.0		$5.0^{+12.26}_{-3.54}$	2.25 ± 0.12	o5;x1
1999-08d	2451400.61	18.3(i')	87.2	Y		710	357 ± 357	753 ± 35		1.2 ± 0.4		$2.02^{+9.49}_{-2.02}$	1.26 ± 0.06	o8,9;x7
1999-10a	2451454.70	17.5(W)		O		403	1256 ± 496	2203 ± 234	spec	21.2 ± 1.6	$34.0^{+4.0}_{-4.0}$	$6.26^{+21.98}_{-4.96}$	3.68 ± 0.39	o10;x2
2000-07a	2451753.00	16.8(R)	22.4	O		1013	162 ± 8	1904 ± 236	spec	13.4 ± 0.7	$33.0^{+5.0}_{-5.0}$	$0.99^{+1.75}_{-0.63}$	3.18 ± 0.39	o8,9;x1
2000-08a	2451719.62	18.6(R)		O		795	278 ± 75	1061 ± 567		16.8 ± 9.7		$1.61^{+4.08}_{-1.16}$	1.77 ± 0.95	o11;x1
2001-01a	2451929.32	17.1(R)		O		328	1989	2426 ± 109		2.6 ± 0.6		9.47	4.05 ± 0.18	o12;x3
2001-07a	2452094.56	18.7(R)		Y		1584	60 ± 60	153 ± 34		5.3 ± 2.0		$0.41^{+1.53}_{-0.41}$	0.26 ± 0.06	o12;x1
2001-08d	2452150.60	16.7(R)	11.8	O		1720	50 ± 13	593 ± 463		0.7 ± 0.1		$0.34^{+0.67}_{-0.23}$	0.99 ± 0.77	o12;x1
2001-10a	2452186.41	17.0(R)	39.3	O	Fe II	430	1089 ± 70	> 2702	spec	39.0 ± 8.0	$14.0^{+4.0}_{-7.0}$	$5.5^{+13.18}_{-3.87}$	> 4.51	o9,13;x2

Table 10. continued.

Optical measurements						X-ray measurements						Derived parameters		Comments
Name M31N	Outburst[a] (JD)	Brightness[b] (mag Filter)	t_{2R} [c] (d)	Old/[d] Young	Type[e]	v_{exp} [f] (km s^{-1})	Turn on (d)	Turn off (d)	SSS?[g]	L_X^h (10^{36} erg s^{-1})	kT_{BB}^i (eV)	Ejected mass (10^{-5} $M_\odot$)	Burned mass (10^{-6} $M_\odot$)	o(ptical)[j] and x(-ray)[k]
2001-10b	2452191.48	15.6(i')	15.8	Y		894	214 ± 214			6.7 ± 2.2		$1.27^{+5.63}_{-1.27}$		o8,9;x7
2001-10f	2452196.26	16.6(B)	12.0	Y		1704	51 ± 34	550 ± 460	spec	37.0 ± 1.7	$48.0^{+11.0}_{-11.0}$	$0.35^{+1.02}_{-0.29}$	0.92 ± 0.77	o14,15;x1,2
2001-11a	2452226.21	17.1(B)	8.0	Y		1675	53			2018.4 ± 246.6		0.36		o15;x8
2002-01b	2452282.31	16.8(R)	8.0	O		**1500**	77 ± 69	534 ± 390		27.5 ± 12.0		$0.51^{+1.85}_{-0.47}$	0.89 ± 0.65	o17,18;x1
2003-08c	2452878.50	17.9(R)		O		**450**	1419 ± 126	> 2010		5.5 ± 1.1		$6.98^{+17.92}_{-5.0}$	> 3.36	o19,20;x14
2003-11a	2452948.47	16.9(R)	22.0	O		739	327 ± 70	709 ± 235		27.6 ± 1.8		$1.86^{+4.54}_{-1.32}$	1.18 ± 0.39	o21,12;x2
2003-11b	2452973.37	17.4(R)	42.2	O		766	302 ± 70	684 ± 235		10.4 ± 1.3		$1.74^{+4.26}_{-1.23}$	1.14 ± 0.39	o12;x2
2004-01b	2453006.24	18.4(R)		O		361	1609 ± 163	> 1882		6.7 ± 1.5		$7.82^{+20.74}_{-5.66}$	> 3.14	o12;x14
2004-05b	2453143.56	17.2(R)	49.7	O		896	213 ± 11	> 1745	spec	45.8 ± 5.4	$30.0^{+6.0}_{-5.0}$	$1.27^{+2.34}_{-0.82}$	> 2.92	o22,11;x2
2004-06a	2453164.54	17.2(R)	19.7	O		1539	64 ± 23	218 ± 16	spec	62.1 ± 9.0	$71.0^{+9.0}_{-9.0}$	$0.43^{+0.97}_{-0.3}$	0.36 ± 0.03	o22,11;x2
2004-06c	2453181.52	17.1(R)	10.9	O		1294	94 ± 70	476 ± 234		33.9 ± 2.0		$0.61^{+2.05}_{-0.53}$	0.8 ± 0.39	o22,11;x2
2004-08a	2453220.47	17.4(R)		O		1752	48 ± 16	77 ± 13	spec	51.9 ± 8.2	$80.0^{+16.0}_{-16.0}$	$0.33^{+0.7}_{-0.23}$	0.13 ± 0.02	o22,11;x2
2004-08c	2453239.54	18.7(R)	50.3	O		1661	54 ± 54	144 ± 16		9.3 ± 1.0		$0.37^{+1.37}_{-0.37}$	0.24 ± 0.03	o12;x2
2004-11f	2453311.82	17.9(R)	28.4	O		2794	17 ± 17	45 ± 10		353.3 ± 6.2		$0.13^{+0.42}_{-0.13}$	0.08 ± 0.02	o12;x2
2004-11b	2453315.35	16.6(R)	32.0	O	Fe II	**1250**	68 ± 16	343 ± 235		16.2 ± 1.6		$0.45^{+0.9}_{-0.3}$	0.57 ± 0.39	o22,11;x2
2004-11g	2453315.35	18.0(R)	28.4	O		2872	16 ± 16	343 ± 235		82.1 ± 3.0		$0.12^{+0.39}_{-0.12}$	0.57 ± 0.39	o22;x2
2004-11e	2453339.30	17.6(R)	34.6	Y		1822	44 ± 16	319 ± 235		35.9 ± 4.0		$0.31^{+0.66}_{-0.21}$	0.53 ± 0.39	o22,11;x2
2005-01b	2453389.58	16.3(W)		Y		808	268 ± 268	804 ± 269	spec	10.0	45.0	$1.56^{+7.08}_{-1.56}$	1.34 ± 0.45	o23;x6
2005-01c	2453399.59	16.1(W)		Y		715	352 ± 352		spec	120.0	$40.0^{+1.0}_{-1.0}$	$1.99^{+9.36}_{-1.99}$		o23;x6
2005-02a	2453420.27	17.7(W)		O		855	236 ± 236	872 ± 121	spec	56.0 ± 5.0	$38.0^{+6.0}_{-8.0}$	$1.39^{+6.22}_{-1.39}$	1.46 ± 0.2	o24;x3
2005-09b	2453614.73	16.5(W)		Y	Fe II	**2200**	150 ± 150	494 ± 195	spec	25.0	60.0	$0.92^{+3.91}_{-0.92}$	0.83 ± 0.33	o25,26;x9,6
2006-04a	2453851.77	15.9(R)	16.0	O		1347	86 ± 19	132 ± 27	spec	51.0 ± 2.0	$54.0^{+9.0}_{-10.0}$	$0.56^{+1.13}_{-0.37}$	0.22 ± 0.05	o27,28;x3
2006-06a	2453877.60	17.6(R)		O	Fe II	**850**	106 ± 26	200 ± 25		10.0 ± 2.0		$0.68^{+1.45}_{-0.46}$	0.33 ± 0.04	o29,26;x3
2006-06b	2453869.57	18.5(R)		O		502	772 ± 138	> 1019	spec	11.0 ± 2.0	$33.0^{+4.0}_{-3.0}$	$4.04^{+10.63}_{-2.92}$	> 1.7	o30,11;x14
2006-09c	2453996.64	17.0(R)	14.0	Y	Fe II	**570**	275 ± 138	327 ± 164	spec	2.8 ± 0.8	$59.0^{+7.0}_{-7.0}$	$1.59^{+5.06}_{-1.27}$	0.55 ± 0.27	o31,32;x14

ble 10. continued.

Optical measurements						X-ray measurements						Derived parameters		Comments
Name M31N	Outburst[a] (JD)	Brightness[b] (mag Filter)	t_{2R} [c] (d)	Old/[d] Young	Type[e]	v_{exp} [f] (km s^{-1})	Turn on (d)	Turn off (d)	SSS?[g]	L_X^h (10^{36} erg s^{-1})	kT_{BB}^i (eV)	Ejected mass (10^{-5} $M_\odot$)	Burned mass (10^{-6} $M_\odot$)	o(ptical)[j] and x(-ray)[k]
2006-11a	2454064.17	16.0(R)	22.0	Y	Fe II	1059	147 ± 41	208 ± 21	spec	19.0	$65.0^{+25.0}_{-25.0}$	$0.91^{+2.12}_{-0.64}$	0.35 ± 0.04	o33,34;x10,11
2007-02b	2454135.30	16.7(R)	37.0	Y	Fe II	**800**	175 ± 175	> 732	spec	18.0 ± 5.0	$28.0^{+11.0}_{-10.0}$	$1.06^{+4.58}_{-1.06}$	> 1.22	o35,36;x14
2007-06b	2454270.40	17.3(W)	18.0	O	He/N	**1500**	87 ± 54	452 ± 57	spec	97.0 ± 12.0	$48.0^{+2.0}_{-3.0}$	$0.57^{+1.71}_{-0.46}$	0.76 ± 0.1	o37;x12,14
2007-10b	2454386.75	17.8(R)	3.0	Y	He/N	**1450**	13 ± 13	92 ± 5	spec	32.0 ± 4.0	$66.0^{+34.0}_{-24.0}$	$0.1^{+0.32}_{-0.1}$	0.15 ± 0.01	o38,39;x14
2007-11a	2454406.78	16.7(R)	4.0	O		3399	11 ± 5	52 ± 7		66.0 ± 4.0		$0.09^{+0.17}_{-0.06}$	0.09 ± 0.01	o40;x0,14
2007-12b	2454444.03	17.0(R)	8.0	Y	He/N	**2250**	25 ± 5	115 ± 55	spec	339.0 ± 4.0	$84.0^{+3.0}_{-2.0}$	$0.18^{+0.3}_{-0.11}$	0.19 ± 0.09	o41,42;x13,14
2007-12d	2454452.07	17.2(R)	4.0	O	He/N	**2750**	17 ± 5	27 ± 5		2.8 ± 0.8		$0.13^{+0.22}_{-0.08}$	0.05 ± 0.01	o43,44;x14
2008-05a	2454601.29	16.4(R)	25.0	O		939	192 ± 5	> 278	spec	11.0 ± 2.0	$45.0^{+25.0}_{-28.0}$	$1.15^{+2.02}_{-0.73}$	> 0.46	o45,11;x14
2008-05b	2454609.26	16.0(W)		O		957	184 ± 6	215 ± 6		4.9 ± 1.3		$1.11^{+1.95}_{-0.71}$	0.36 ± 0.01	o45,11;x14
2008-06a	2454631.96	17.7(R)		O		831	252 ± 5	> 252		3.2 ± 1.3		$1.47^{+2.67}_{-0.95}$	> 0.42	o46;x14

otes: [a]: Julian day of optical nova outburst; [b]: maximum observed magnitude, "W" indicates unfiltered magnitude; [c]: time in days the nova R magnitude needs to drop 2 mag below peak magnitude e Payne-Gaposchkin 1964); [d]: positional association with the old (bulge) and young (disk) stellar populations of M 31 (see Sect. 5.5) ; [e]: spectral type of optical nova according to the classification heme of Williams (1992); [f]: outflow velocity of the ejected envelope, values in *bold face* are measured from optical spectra, all other values were computed from the SSS turn-on time using Eq. 5; [g]: dicates if the source was classified as a SSS using XMM-Newton spectra (spec), XMM-Newton hardness ratios (HR), *Chandra* HRC-I/ACIS-I hardness ratios (HR1), *Chandra* HRC-I hardness ratios R2), or a ROSAT observation (ROSAT) in the case of M31N 1990-09a; [h]: unabsorbed luminosity in 0.2–1.0 keV band in units of 10^{36} erg s^{-1} during observed maximum X-ray brightness assuming a eV blackbody spectrum with Galactic foreground absorption; [i]: maximum blackbody temperature from spectral fits; [j]: optical references: o1: Ciardullo et al. (1987), o2: Nedialkov et al. (2002), o3: after & Irby (2001), o4: Ansari et al. (2004), o5: Rector et al. (1999), o6: Henze et al. (2008b), o7: Sharov & Alksnis (1998), o8: Darnley et al. (2004), o9: Darnley et al. (2006), o10: Filippenko et al. 999), o11: CBAT M 31 nova webpage (http://www.cfa.harvard.edu/iau/CBAT_M31.html), o12: MPE M 31 nova catalogue (http://www.mpe.mpg.de/~m31novae/opt/m31/index.php), o13: Filippenko Chornock (2001), o14: Smirnova & Alksnis (2006), o15: Alksnis et al. (2008), o16: Smirnova et al. (2006), o17: Fiaschi et al. (2002), o18: Filippenko & Chornock (2002), o19: Fiaschi et al. (2003), 0: di Mille et al. (2003), o21: Hornoch (2003), o22: PHS2007 , o23: D. Bishops extragalactic nova webpage (http://www.supernovae.net/sn2005/novae.html), o24: Dimai & Manzini (2005), o25: uimby et al. (2005), o26: Pietsch et al. (2006a), o27: Pietsch et al. (2006b), o28: Baernbantner & Riffeser (2006), o29: Lang et al. (2006), o30: Ries (2006), o31: Quimby (2006), o32: Shafter et al. 006), o33: K. Hornoch (2010, priv. comm.), o34: A. Shafter's webpage of nova spectra (http://mintaka.sdsu.edu/faculty/shafter/extragalactic_novae/HET/index.html), o35: Burwitz et al. (2010, in ep.), o36: Pietsch et al. (2007a), o37: Shafter & Quimby (2007), o38: Burwitz et al. (2007), o39: Rau et al. (2007), o40: Pietsch et al. (2007b), o41: Bode et al. (2009), o42: Shafter (2007b), o43: nze et al. (2007), o44: Shafter (2007a), o45: Henze et al. (2008c), o46: Henze et al. (2008a); [k]: X-ray references: x1: PFF2005 , x2: PHS2007 , x3: Paper I , x4: Nedialkov et al. (2002), x5: Pietsch al. (2006c), x6: Stiele et al. (2010), x7: Nelson et al. (2008a), x8: Smirnova et al. (2006), x9: Orio & Nelson (2008) (wrongly named 2005-09c there), x10: Pietsch et al. (2007c), x11: Voss et al. 008), x12: Henze et al. (2009a), x13: Pietsch et al. (2010, in prep.), x14: this work.

5. Discussion

5.1. Novae with long SSS states - sustained hydrogen burning through re-established accretion?

In our monitoring we detected six X-ray counterparts of optical novae that are still active for about five to twelve years after the optical outburst. These novae are M31N 1996-08b, M31N 1997-11a, M31N 2001-10a, M31N 2004-05b (all described in Sect. 3.1), M31N 2003-08c and M31N 2004-01b (see Sect. 3.2). They are all visible at the end of the 2008/9 monitoring for 12.5, 11.0, 7.4, 4.8, 5.5 and 5.2 years after the optical outburst, respectively (see Tables 4 and 5).

Novae M31N 2003-08c and M31N 2004-01b are relatively faint sources ($L_x \sim 5{\times}10^{36}$ erg s^{-1}) that were detected for the first time in our 2007/8 and 2008/9 campaign, respectively. Both sources show variability by at least a factor of two (see Table 5) but there is no indication of a decline in luminosity over time. All of the remaining four novae were already detected by PHS2007 and were also found in our 2006/7 monitoring campaign described in Paper I. Of these four SSSs only M31N 1997-11a shows a declining light curve over the course of the three monitoring campaigns described in Paper I and in this work. The X-ray luminosity of the other three nova counterparts exhibits on average no significant change from 2007 to 2009.

This long-term behaviour of the source luminosity is not compatible with a cooling post-nova WD, the luminosity of which should decrease over time after the outburst (see e.g. Prialnik 1986). Therefore, we speculate that re-established hydrogen accretion in the binary system might be prolonging the nuclear burning on the WD surface that was initiated by the nova outburst. A similar scenario was discussed by Ness et al. (2008) for the Galactic nova V723 Cas which has the longest SSS phase known so far (more than 14 years in 2009; Schaefer & Collazzi 2010). Note, that M31N 1996-08b is the current runner-up in this hierarchy, followed by M31N 1997-11a and the Galactic nova GQ Mus (SSS turn-off after 10 years; Schaefer & Collazzi 2010; Shanley et al. 1995).

Recently, Schaefer & Collazzi (2010) introduced a new subclass of Galactic novae which they named "V1500 Cyg stars" after its prototype. The members of this subclass share five distinct properties, one of which is a long-lasting SSS phase. The other four are (i) a short orbital period, (ii) a highly magnetised WD, (iii) an optical post-eruption magnitude significantly brighter than the pre-eruption magnitude and (iv) a slow optical decline after outburst. To explain the connection between these properties, Schaefer & Collazzi (2010) discussed a physical model which essentially involves magnetically channelled, irradiation enhanced accretion onto the WD from its nearby companion star to produce prolonged SSS emission (see also Warner 2002).

It would be interesting to examine if some of the M 31 novae discussed here might be V1500 Cyg stars as well. Unfortunately, M 31 is too far away to meassure optical magnitudes of novae in quiescence. The typical absolute (B) magnitude of a nova at quiescence is $M_B \sim +4.5$ mag and the extinction free distance modulus is of M 31 is $\mu_0 = 24.38$ mag (Freedman et al. 2001). Furthermore, our X-ray light curves do not show periodicities that might reveal the orbital period of the system or point towards a magnetic WD. However, since the novae discussed here are faint X-ray sources, maybe with the exception of M31N 2004-05b (the short-term X-ray light curves of which do not show periodic variations), we cannot exclude either property. This leaves us with the speed of optical decline and indeed we find that both M31N 2001-10a and M31N 2004-05b have relatively long $t_{2,R}$ decay times, of 39.3 and 49.7 days, respectively (see Table 10). While we have not enough information to decide whether any of these novae could be a V1500 Cyg star, it is worth mentioning that their long SSS phase could be explained in the framework of this subclass (Schaefer & Collazzi 2010).

Another piece of evidence for re-established accretion in four of the novae (M31N 1997-11a, M31N 2004-05b, M31N 2003-08c and M31N 2004-01b) is the presence of significant variability on short time scales in their X-ray light curves. For M31N 1997-11a the luminosity increased by about a factor of two from *Chandra* observations 8528 to 8529 and returned to its previous state in observation 8530. For M31N 2004-05b we noticed a similar phenomenon between observations 8526, 8527 and 8528 (see Table 4). The observations are separated by about ten days (see Table 1). The variability of M31N 2003-08c is difficult to constrain, because the source is only slightly above the detection limit in most cases. The luminosity of nova M31N 2004-01b increased significantly towards the end of the 2008/9 campaign. Long after the nova outburst, there should be no significant variability present in the light curve of a cooling WD. Our observations might therefore reveal variability caused by accretion.

At this stage, we are still left with little more than speculation about what may cause the extraordinary length of the SSS state in these six novae. However, if re-established accretion in these systems is providing enough hydrogen fuel to prolong the SSS phase significantly, then the lower limits for the burned mass derived from this extended SSS phase (see Table 10 and Eq. 8) are not constraining the hydrogen mass that was left on the WD after the nova outburst. Finally, there is the possibility that faint SSSs like XMMM31 J004318.7+411804 (see Sect. 3.4 and Table 9), which shows a light curve similar to that of M31N 2003-08c, might be novae with a long SSS phase for which the optical outburst has been missed due to monitoring gaps.

5.2. Correlations between nova parameters

The nova SSS catalogue compiled in Table 10 was used to search for statistical correlations between the various X-ray and optical observables. Here we present correlations that were found between the following parameters: turn-on time ($t_{\rm on}$), turn-off time ($t_{\rm off}$), effective temperature kT (all X-ray), t_2 decay time and expansion velocity of the ejected envelope (both optical). The correlations are shown in Figs. 12 – 16. To model the visible trends we used a least-square fit with a power law, the results of which are given Eqs. 2 – 5.

We assume that the physical parameter mainly responsible for the various correlations is the WD mass. Also in optical studies the WD mass was found to be the dominating parameter (see e.g. Livio 1992; Della Valle & Livio 1995; Della Valle 2002, and references therein). However, theoretical nova models show a more complicated picture (see e.g. Sala & Hernanz 2005; Hachisu & Kato 2006) and we included a note of caution about the physical interpretation of our correlations.

While a detailed interpretation of the observed correlations is beyond the scope of this paper we believe that our analysis revealed certain trends between different nova parameters that might be used as input for future theoretical models. In the following, we describe the correlations found.

5.2.1. SSS turn-on time vs turn-off time

We plot the two X-ray time scales $t_{\rm on}$ vs $t_{\rm off}$ in Fig. 12. There is a trend correlating increasing turn-on times with increasing turn-

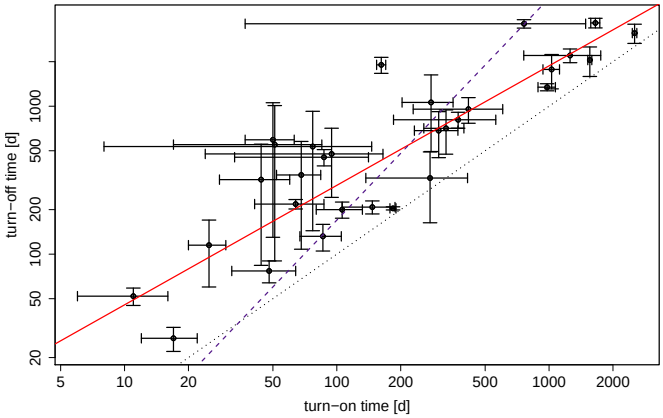

Fig. 12. Double logarithmic plot of turn-on time versus turn-off time (both in days after outburst) including error bars. The solid red line represents the best fit from a weighted regression. The dashed purple line shows the $t_{\rm off}$ vs $t_{\rm on}$ relation of Hachisu & Kato (2010). The dotted black line indicates the limiting case of $t_{\rm off} = t_{\rm on}$.

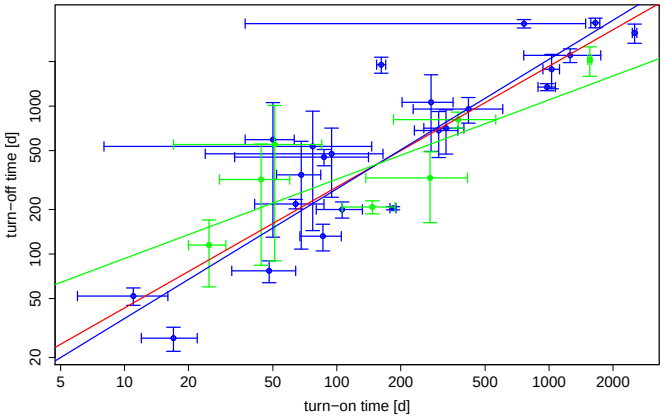

Fig. 13. Same as Fig. 12, here with different colours of symbols and best-fit lines for old novae (associated with bulge stellar population; **blue**) and young novae (disk population; **green**). The red line still shows the overall best fit.

off times. Note, that because of the definition of both times it is not possible that $t_{\rm off} \leq t_{\rm on}$. The limiting case of $t_{\rm off} = t_{\rm on}$ is shown as a dotted black line in Fig. 12. However, the correlation that we see is much more specific than $t_{\rm off} > t_{\rm on}$ and can be fitted with a powerlaw model. This model is shown as the solid red line in Fig. 12 and defined by the following relation (both time scales in units of days after outburst):

$$t_{\rm off} = 10^{(0.9\pm0.2)} \cdot t_{\rm on}^{\ (0.8\pm0.1)} \quad . \tag{2}$$

This dependence is significantly less steep than the relation between $t_{\rm on}$ and $t_{\rm off}$ inferred from a prediction formula of the SSS phase of novae recently published by Hachisu & Kato (2010). From their equations 25 and 26 one can derive that $t_{\rm off} \propto t_{\rm on}^{1.5}$. This relation is shown as the dashed purple line in Fig. 12.

Separate modelling of novae from young and old stellar populations (see Sect. 5.5) indicates a difference in the model slope (see Fig. 13). The slope for old novae is 0.88 ± 0.10 (blue line in Fig. 13) and for young novae 0.54 ± 0.18 (green line in Fig. 13).

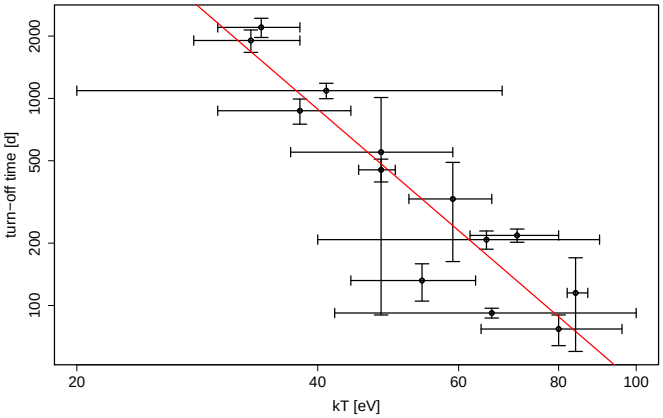

Fig. 14. Double logarithmic plot of effective temperature (kT) in eV versus turn-off time in days after outburst including error bars. The red line represents the best fit from a weighted regression.

However, this difference is significant only on the 1σ level and an analysis of covariance does not show a significant impact of the type of population on the model. Since this result is strongly influenced by the small number of young novae, a larger sample is needed to study the difference further.

5.2.2. Effective black body temperature vs X-ray time scales

We plot the effective black body temperature kT vs the SSS turn-off time $t_{\rm off}$ in Fig. 14. The figure shows an anti-correlation of these two X-ray parameters. We fitted this trend with a power-law, which is represented by the solid red line in Fig. 14. The fit indicates the following relation, where the turn-off time is given in units of days after outburst and the effective temperature in units of eV:

$$t_{\rm off} = 10^{(8.3\pm0.7)} \cdot kT^{(-3.3\pm0.4)} \quad . \tag{3}$$

In order to interpret this relation physically, we made use of a result from theoretical models which states that higher effective temperatures indicate a larger WD mass (see e.g. figure 7 in Sala & Hernanz 2005). It is therefore tempting to speculate that Eq. 3 represents a relation between WD mass and turn-off time. This relation might be similar to the one shown in figure 9(a) of Hachisu & Kato (2006), where they plot the WD mass versus the time when hydrogen-burning ends (which is generally agreed on to correspond to the SSS turn-off time). One caveat in establishing such a relation is that figure 7 in Sala & Hernanz (2005) is given for the *maximum* effective temperature which might not be the same as the blackbody kT derived from our observations. First, because blackbody fits to supersoft spectra are not physically correct representations of an evolving WD atmosphere and are generally known to underestimate the source temperature (see Sect. 1). Second, because our observations might not detect the SSS at its maximum temperature. However, the trend visible in Fig. 14 shows that our simple blackbody parametrisation seems capable of at least distinguishing between high temperature and low temperature SSSs. Furthermore, figures 10 and 11 in Sala & Hernanz (2005) show that novae evolve quickly through the low kT phase in their SSS state and spend most of the time close to their maximum effective temperature. Finally, we repeated the regression for old novae and young novae separately (see Sect. 5.5) but did not find significant differences.

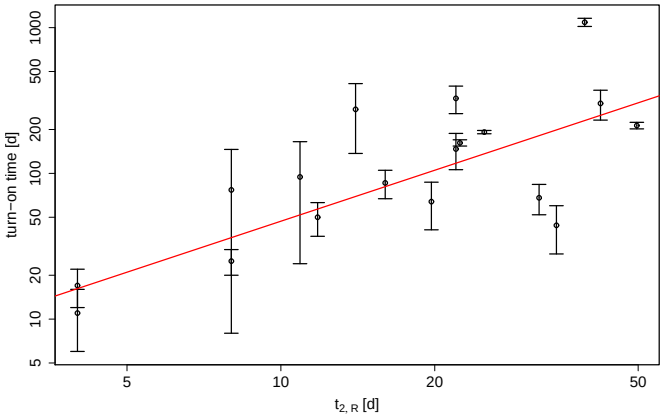

Fig. 15. Double logarithmic plot of optical decay time $t_{2,R}$ versus turn-on time (both in units of days after outburst) including error bars. The red line represents the best fit from a weighted regression.

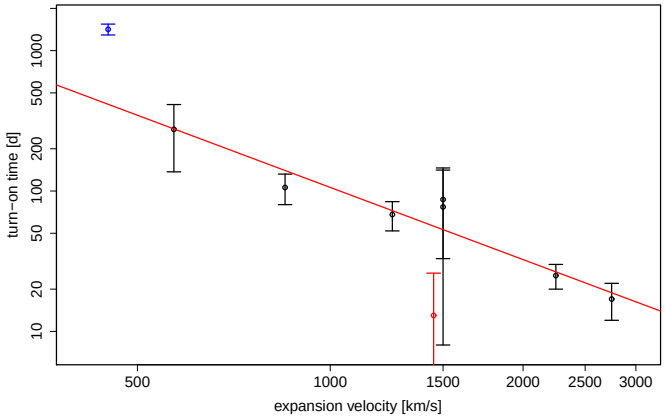

Fig. 16. Double logarithmic plot of expansion velocity in km s^{-1} versus turn-on time in days after outburst including error bars. The red line indicates the best fit from a weighted regression. The red data point represents the atypical nova M31N 2007-10b. The blue data point is nova M31N 2003-08c for which the actual turn-on time is difficult to determine.

5.2.3. Optical decay time vs SSS turn-on time

We plot the time of optical decay by two magnitudes in the R band ($t_{2,R}$) vs the SSS turn-on time in Fig. 15. Note, that only from optical R band light curves there is sufficient data to perform a statistical analysis. The plot indicates a trend that is positively correlating the two parameters. We modelled this correlation with a powerlaw, which is indicated as a red line in Fig. 15. The model gives the following relation:

$$t_{\rm on} = 10^{(0.5\pm0.3)} \cdot t_{2,R}^{\ (1.2\pm0.2)} \quad . \tag{4}$$

Both time scales are in units of days after nova outburst. We therefore obtain a roughly linear relation between the two important timescales in optical and X-ray. However, the scatter of the data points in Fig. 15 is relatively large and a few data points lie significantly off the powerlaw model. This behaviour might indicate a more complex relation between the two time scales that should be further examined in future studies using a larger nova sample.

Note, that from their theoretical models which are based on observations of Galactic novae Hachisu & Kato (2010) recently derived a relation between t_2 and the turn-on time which is also linear but much steeper (their equation 30 combined with 29). This discrepancy might be due to the fact that Hachisu & Kato (2010) used decay times in the emission line free optical y band, whereas our results depend on R band light curves. The continuum flux of a nova in this band is contaminated by the Hα emission line, which is the most prominent characteristic of a nova spectrum. Observers have used the fact that novae are visible longer in Hα since the work of Ciardullo et al. (1983).

5.2.4. Optical expansion velocity vs SSS turn-on time

We plot the expansion velocity of the ejected envelope ($v_{\rm exp}$), as measured from optical spectra, vs the SSS turn-on time ($t_{\rm on}$) in Fig. 16. This diagram includes all novae for which $v_{\rm exp}$ is known and $t_{\rm on}$ had been measured accurately enough. It shows an anti-correlation trend between both parameters.

Before we modelled this trend we excluded two novae, which are colour coded in Fig. 16: M31N 2003-08c (blue) and M31N 2007-10b (red). M31N 2003-08c has a luminosity close to our detection limit and is only found in half of the *Chandra* observations during both campaigns (see Table 5). Because of its faintness, the turn-on time of the source is difficult to determine. M31N 2007-10b seems to be a peculiar nova, since already Rau et al. (2007) noted the atypically low expansion velocity (for He/N novae) of 1450 ± 100 km s^{-1}.

The powerlaw model that describes the correlation between the remaining data point is indicated by a red line in Fig. 16 and described by the following relation:

$$t_{\rm on} = 10^{(7.1\pm0.8)} \cdot v_{\rm exp}^{\ (-1.7\pm0.2)} \tag{5}$$

The turn-on time is given in units of days after nova outburst and the expansion velocity in units of km s^{-1}. This model is based only on a few objects for which both quantities are known. Nevertheless, the scatter is small and the correlation is strong, with a Pearson correlation coefficient of -0.96 and a non-correlation p-value of 0.0008. Note, that the uncertainty ranges of the expansion velocities are not available in the literature in most of the cases of Table 10. However, from what we know these errors are in the range of 10% and are therefore not expected to strongly influence the derived relation.

Another caveat is that expansion velocities of novae are known to be time dependent. Hatzidimitriou et al. (2007) found for the optical nova M31N 2005-09c (no SSS counterpart known) a decline in Hα of about 200 km s^{-1} within six days. However, there is no explicit relation between expansion velocity and time after nova outburst known so far. Of the eight nova that we used to derive Eq. 5, only for three the optical spectrum has not been taken within the first six days after outburst. Assuming a decline in expansion velocity over time, correcting for this delay would decrease the slope of the best fit.

The implications of the trend visible in Fig. 16 are intuitively clear: larger expansion velocities should result in shorter turn-on times of the SSS, because the ejected envelope becomes optically thin earlier. Equation 5 quantifies this correlation. It connects the two parameters needed to compute ejected masses (see Table 10) and could allow us to estimate these masses with higher accuracy (see Sect. 5.3). Furthermore, it could allow the estimation of the SSS turn-on time from the optical spectrum and therefore it could be an important tool for planning X-ray observations of optical novae.

5.2.5. Physical interpretations - a note of caution

At this point, a general note of caution is in order: Theoretical models emphasise that the properties of a nova outburst are not only influenced by the mass of the WD, but also by its chemical composition (mainly the hydrogen content of the envelope, see e.g. Sala & Hernanz 2005; Hachisu & Kato 2006). This additional dependence is not accounted for in any of the simple power-law relationships presented here. However, according to the theoretical models the impact of the chemical composition on the observed parameters appears to be considerably weaker than the influence of the WD mass: see e.q. figure 9 in Hachisu & Kato (2006) and figure 7 in Sala & Hernanz (2005). In particular, the effect of the chemical composition on kT in figure 7 of Sala & Hernanz (2005) (WD mass versus maximum effective temperature) seems to be in the same range ($\sim$ 15 eV) as the scatter and the error bars for kT in our Fig. 14 (effective temperature versus turn-on time). Therefore, there is the possibility that most of the impact from parameters other than the WD mass on the correlations found in this work is still within the range of the (still relatively large) error bars. As to which extend the varying hydrogen content itself might be causing the observed scatter in the correlations might be an interesting question for further studies.

5.3. Derived nova parameters

In addition to the observed parameters of the optical nova and the X-ray counterpart, our catalogue (see Table 10) also contains the derived parameters, ejected hydrogen mass ($M_{\rm ej,H}$) and burned hydrogen mass ($M_{\rm burn,H}$).

The mass of hydrogen ejected in a nova outburst can be estimated from the turn-on time of the SSS and from the expansion velocity of the ejected material. Under the assumption of a spherical symmetric nova shell (Della Valle et al. 2002), the column density of hydrogen evolves with time as

$$N_H(\mathrm{cm}^{-2}) = M_{\rm ej,H}/(\frac{4}{3}\pi \cdot m_H \cdot v_{\rm exp}^2 \cdot t^2 \cdot f') \quad , \qquad (6)$$

and the SSS turns on at $t = t_{\rm on}$ when $N_{\rm H}$ decreases to $\sim 10^{21}$ cm^{-2}. Here, $m_H = 1.673 \times 10^{-24}$ g is the mass of the hydrogen atom and $f' \sim 2.4$ a geometric correction factor (see Paper I). The newly found correlation between SSS turn-on time and expansion velocity given in Eq. 5 now allows us to eliminate the expansion velocity from this relation. We can therefore compute the ejected mass solely from the SSS turn-on time. This allows more accurate mass and error range estimates for the vast majority of novae without an optical spectrum. Although Eq. 5 is only based on a few objects, it is an improvement compared to earlier work, where ejected masses had to be computed using a "typical" expansion velocity with unknown errors (see e.g. Paper I). Ejected hydrogen masses and error ranges in Table 10 were computed as follows, with $a = 10^{8.4\pm0.2}$ being a correlation coefficient derived from inserting Eq. 5 into Eq. 6 for $t = t_{\rm on}$:

$$M_{\rm ej,H} = N_H \cdot \frac{4}{3}\pi \cdot m_H \cdot f' \cdot a \cdot {t_{\rm on}}^{(1.1\pm0.1)} \qquad (7)$$

This equation was also used for novae with known expansion velocities. Because of the tight correlation seen in Fig. 16, for these novae there are no big differences between computed and measured $v_{\rm exp}$.

The amount of hydrogen mass burned on the WD surface is computed as in Paper I:

$$M_{\rm burn,H} = (L_{\rm bol} \cdot t_{\rm off})/(X_H \epsilon) \quad , \qquad (8)$$

where $L_{\rm bol}$ is the bolometric luminosity, $t_{\rm off}$ the SSS turn-off time, X_H the hydrogen fraction of the burned material, and $\epsilon = 5.98 \times 10^{18}$ erg g^{-1} (Sala & Hernanz 2005). As in Paper I we use a constant bolometric luminosity of $3{\times}10^4 L_\odot$ and a hydrogen mass fraction of $X_H = 0.5$ (for a discussion of these parameter values see Paper I).

Despite the uncertainties, the burned masses presented in Table 10 are within the range expected from models of stable envelopes with steady hydrogen burning (Sala & Hernanz 2005; Tuchman & Truran 1998). In general, the burned masses are about one order of magnitude smaller than the ejected masses, which for most novae are within the values predicted from hydrodynamical models of nova outbursts (José & Hernanz 1998). Note, that in the scenario of sustained H-burning through re-established accretion (see Sect. 5.1) the burned masses computed for novae with long SSS states only constitute upper limits on the actual hydrogen mass left on the WD after the outburst.

5.4. SSS phase duration in novae and the completeness of the X-ray monitoring

In previous studies it had been noticed that only a minor fraction of novae in M 31 were actually observed as SSSs. While PHS2007 detected SSS emission from 11 out of 32 novae within about a year after optical outburst, in Paper I only 2 out of 25 novae were found in X-rays over a comparable time span. For the current work the corresponding numbers are 6 out of 28 (2007/8) and 3 out of 23 (2008/9) novae, respectively.

Based on current theoretical models, all novae are expected to display a SSS phase (see e.g. Hachisu & Kato 2010). Therefore, the cause of the low percentage of actual detections remained an open question. It could be (a) due to the inevitably incomplete observational coverage, or (b) due to some inadequacy (or incompleteness) of the theoretical models.

Using our nova SSSs catalogue (see Table 10) we could test scenario (a) for the first time. This study strongly benefited from the large number of optical novae found in M 31 over the last 15 years and from the large number of archival and monitoring X-ray observations covering the M 31 central area.

The main steps of our approach were the following: We took the observed mass distribution of WDs in novae as known from theoretical work, converted it into a distribution of SSS turn-on times, "convolved" it with our observational coverage and compared the expected number of detections to the actual observed number of SSS novae using a Monte Carlo Markov Chain (MCMC) method. The entire procedure is explained in detail in the following paragraphs and the results are discussed.

Our starting point was the observed mass function of WDs in CNe which we computed based on Truran & Livio (1986). This approach assumes a Salpeter IMF $\Phi(M) \propto M^{-2.35}$ (Salpeter 1955) for the WD progenitors and computes the nova recurrence frequency as $\nu_{\rm rec} \propto M_{\rm WD}/R_{\rm WD}^4$ based on the critical envelope mass needed to trigger the nova explosion (for more details see Truran & Livio 1986). The intrinsic mass distribution of WDs has its strongest peak at low masses around $0.6 M_\odot$ (see e.g. Catalán et al. 2008, and references therein). However, the WD mass dependence of the recurrence frequency leads to a much higher *observed* frequency of high mass WDs in CNe (see also Ritter et al. 1991).

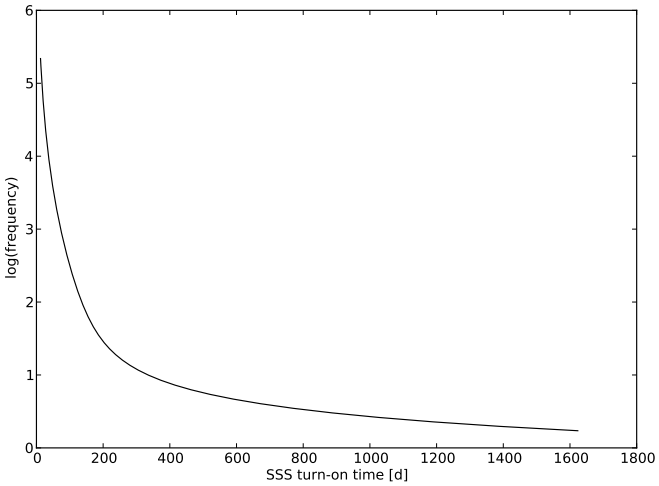

Fig. 17. Expected logarithmic frequency of SSS turn-on times in CNe based on Truran & Livio (1986) and Hachisu & Kato (2006)

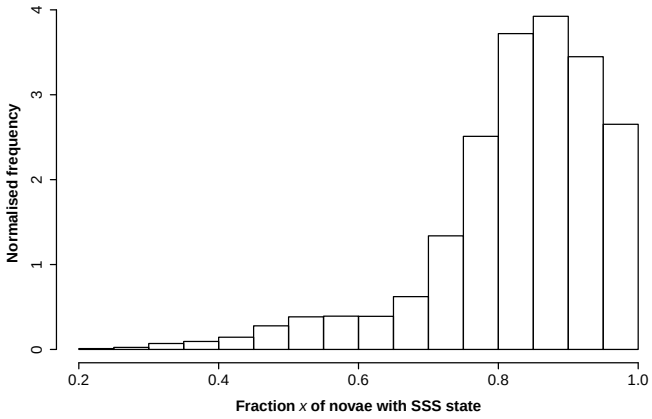

Fig. 18. Result from a MCMC simulation based on the intrinsic distribution of SSS turn-on times for novae in M 31. Shown is the frequency distribution of the intrinsic fraction x of novae with SSS emission which would be needed to cause the detections in our observation campaigns.

In order to translate the expected observed WD mass distribution into an expected observed distribution of SSS turn-on times we used the theoretical models of Hachisu & Kato (2006). These authors computed SSS turn-on and turn-off times for different WD masses and chemical compositions based on a free-free emission model. We used their model values for CO WDs and $X_H = 0.45$ (their table 4; $t_{\rm wind}$ corresponds to $t_{\rm on}$) because it is closest to our assumptions in this paper. Moreover, figure 9 in Hachisu & Kato (2006) shows that the impact of choosing different WD chemical parameters is not huge and thus would not introduce significant errors to our analysis. The values between the grid points in their model were interpolated using a polynomial function. In Fig. 17 we show the resulting expected observed distribution of SSS turn-on times, which is clearly dominated by fast SSSs.

Our method is based on all optical novae discovered in M 31 from 1995 until February 2009, the end of our 2008/9 campaign. From this data set we selected all novae in the field of view of our XMM-Newton/*Chandra* M 31 centre monitoring. To account for the fact that XMM-Newton observations suffer from source confusion in the innermost arcminute around the M 31 centre, we exclude novae from this region. The resulting sample consists of 206 objects. Using a Monte Carlo method we randomly selected SSS turn-on times for a certain fraction x of these novae based on the expected turn-on distribution described above. To compute the associated SSS turn-off times we used the correlation found in our catalogue (see Eq. 2). This resulted in a certain time span of SSS visibility for the selected fraction of novae. The fraction x was the free parameter to be optimised by the MCMC, thereby allowing us to test the scenario (a) outlined above.

We now made use of the large number of M 31 centre observations to estimate discovery rates for the simulated SSSs. These observations include the two monitoring campaigns this paper is based on (see Table 1), the monitoring campaign described in Paper I (their table 1) and the archival XMM-Newton and *Chandra* HRC-I observations analysed by PHS2007 (their tables 2 and 3) and PFF2005. From PFF2005, we only used the XMM-Newton centre observations (c1 - c4 in table 1 of Pietsch et al. 2005b) and the long *Chandra* observations 1912 and 1575. The other observations analysed by PFF2005 were either not pointed at the M 31 centre or only had a short exposure time, and are therefore not useful for this simulation. In total, there are 48 individual observations covering 8.7 years. In the context of the simulation, the SSS counterpart of a nova is defined as detected if there is at least one observation between SSS turn-on time and turn-off time. This somewhat ideal assumption is nonetheless justified by the fact that SSS counterparts of novae are expected to have a bolometric luminosity close to the Eddington limit of the WD (Hernanz 2005), which is between $6{\times}10^{37}$ erg s^{-1} and $2{\times}10^{38}$ erg s^{-1} for WD masses between 0.5 and 1.4 solar masses. If we assume that most of that luminosity is emitted in the soft X-ray band and take into account our typical observational sensitivities of a few 10^{36} erg s^{-1} (see e.g. Table 8), our actual detection efficiency should be close to 100%.

Using the MCMC, SSS turn-on and turn-off times were determined for all novae and the number of sources with detected SSS phase was measured for each of the five campaigns separately. These predicted numbers were then compared to the actual number of novae detected as SSSs in PFF2005 (10) PHS2007 (14), Paper I (8), 2007/8 (11) and 2008/9 (9) for the epoch and spatial region selected above. The deviations between prediction and observation were summed up quadratically to create an error for the estimate. The Markov chain is governed by a Metropolis algorithm (Metropolis et al. 1953) that seeks to minimise this error by modifying the fraction x of novae that gets turn-on times assigned to. The random walk nature of the MCMC allowed us to find the fraction associated with the minimum error and to sample the parameter space around it.

We show the result of the simulation in Fig. 18, where the frequency distribution of the SSS fraction x is plotted. This graph shows that our observational findings are consistent with the assumption that all novae exhibit a SSS stage and that the incomplete observational coverage is the reason for the detection of only a part of them. This result further highlights the importance of novae with high mass WDs and very short SSS turn-on times, which was first found by PHS2007. According to our simulations the intrinsic observed WD mass function strongly favours novae with short SSS states which are expected to account for the majority of the observed sources.

Indeed, we find already five novae with fast SSS turn-on times in the 2007/8 campaign. Their light curves are shown in Fig. 11. A particularly interesting object from this sample is M31N 2007-12d. This nova showed a very short SSS phase and was only detected as a faint source in one observation (see

Table 5). An object like this would have been very likely missed in a sparser sampling. Even in our ten day monitoring it is very close to the detection limit. Therefore, M31N 2007-12d might indicate the lower limit of SSS durations that we are still able to detect with the monitoring strategy applied in this paper.

5.5. Nova population study

The existence of two different nova populations, associated with the bulge and disk of a spiral galaxy, was first postulated based on optical data of Galactic novae (Duerbeck 1990; Della Valle et al. 1992; Della Valle & Livio 1998). Slow Fe II novae were found to be located preferably in the bulge, whereas the faster He/N novae (see Williams 1992, for the spectral classification) mostly belong to the disk. This suggests an association of fast (slow) novae with the overall young (old) stellar population in the disk (bulge). The size and spatial coverage of our nova catalogue, presented in Table 10, for the first time allowed us to investigate the X-ray properties of novae belonging to these two populations in M 31.

Our approach was two-fold. First, we used geometric parameters to distinguish between bulge (old population) and disk (young population) and examined the differences in the distributions of the individual nova parameters for both subsets. Second, we used the X-ray parameters of all novae to divide them into two groups of novae with massive or less massive WDs and tested their geometric distributions. While the first method assumes the existence of two different nova populations, as suggested from optical data, the second method is independent of this assumption. By comparing both approaches, we hoped to correct for selection biases that either of them might introduce. However, in both approaches we applied a geometric criterion and have to be aware that because of the high inclination of M 31 (77.5°; see e.g. Beaton et al. 2007) a significant number of novae occurring in the disk will be projected onto the bulge.

For the first approach, in order to assign a nova to one of the two populations we used an entirely geometrical criterion. We followed the work of Beaton et al. (2007), who analysed NIR images of M 31, and defined the projected M 31 bulge as an ellipse with a semimajor axis of 700″, an ellipticity of 0.5, and a position angle of $\sim 50°$. The boundary between the bulge and disk regions is marked by a grey ellipse in Fig. 19. In the context of this approach, old novae are defined as situated within this boundary and young novae lie outside of it. In Fig. 19 we show the positions of X-ray detected old novae as white and young novae as black crosses, respectively. Note, that we classified nova M31N 2007-06b as a "old nova", the position of which is indicated by the only white cross outside the grey ellipse in Fig. 19. This object was found to be a nova in a M 31 globular cluster (see Shafter & Quimby 2007; Henze et al. 2009a), and therefore belongs to a stellar population similar to the one dominating in the bulge.

We checked the observed distributions of the X-ray parameters given in Table 10 for dependencies on the classification as old or young nova. Only for the black body temperature kT we found significant differences. In Fig. 20 we show the individual kT distributions for young and old novae, respectively. Both distributions are close to Gaussian, with Kolmogorov-Smirnov (KS) test p-values of ~ 0.97, but have different mean values of 42 eV (old) and 55 eV (young). We performed a two sample t-test which gives a p-value of ~ 0.1 for 20 degrees of freedom, resulting in a $\sim 90\%$ probability that the two distributions are different. An F test shows that both variances are equal on the 1σ level (p-value = 0.79) and that the t-test is therefore justified. However, the samples of both old and young novae with measured temperatures (13 and 9) are small. Indeed, statistical power calculations show that if the measured difference in kT between the samples actually is 13 eV we would need at least 28 novae in each group to see a difference on the 95% confidence level (with a power of 0.8).

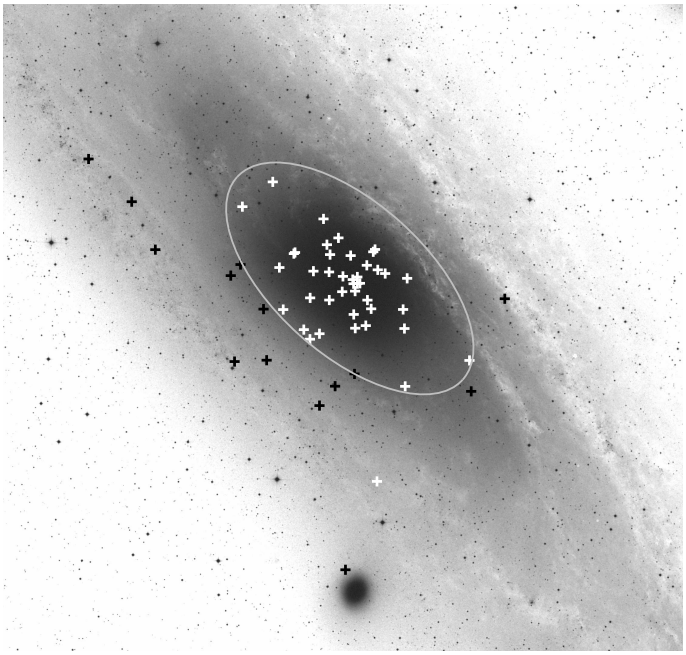

Fig. 19. Location of the M 31 old (white) and young novae (black) overlaid on a DSS2-R image. The grey ellipse marks the boundary between the M 31 bulge and the disk that was used in this work. See Sect. 5.5 for an explanation of the classification. Only four of the 60 nova SSSs from Table 10 are outside this image.

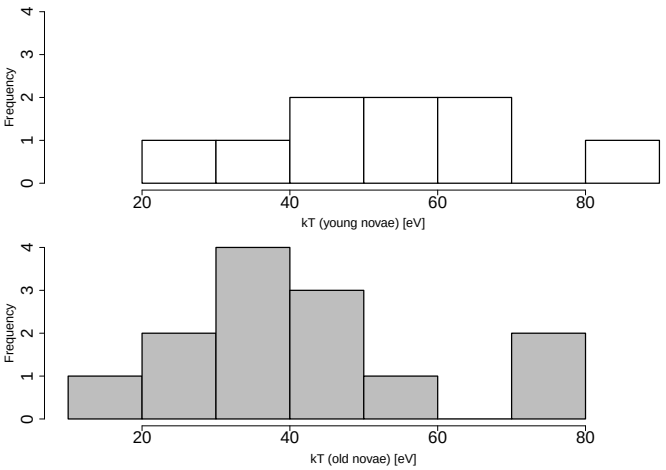

Fig. 20. Distribution of effective (black body) temperature kT for young novae (white/upper panel) and old novae (grey/lower panel), respectively.

In order to examine how much the result obtained above depends on our selection of the boundary between bulge and disk, we tested the method outlined above for different bulge extensions. In Fig. 21 we display the results depending on the semi-major axis of the bulge region. For this computation, we took into account the effect of changing ellipticity in the NIR isophotes of M 31 (see Beaton et al. 2007, their figure 3). The figure shows the t-test p-values for the kT distributions of the

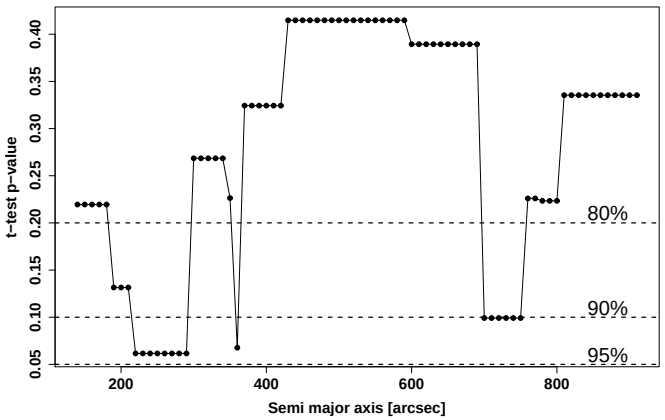

Fig. 21. Two sample t-test p-values for the *kT* distributions of old and young novae. The abscissa gives the semi-major axis of the "bulge" region with is defined to contain the old novae. The solid line connects the solid circles of the data points for better readability. Dashed lines show three acceptance levels for the t-test.

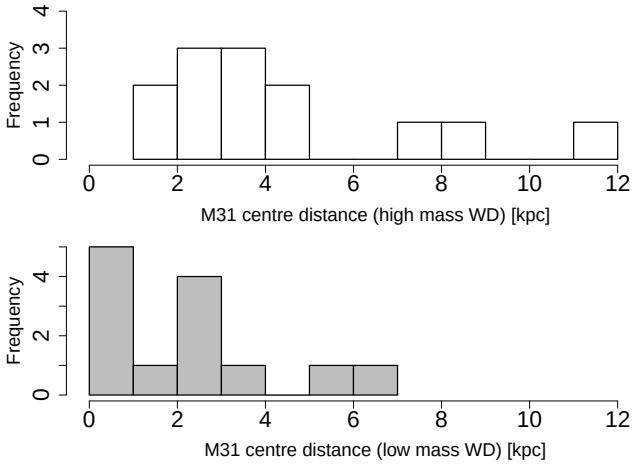

Fig. 22. Distribution of inclination corrected M 31-centric distances for novae with high mass (upper panel, white) and low mass (lower panel, grey) WDs. Distances are given in kpc, assuming a distance to M 31 of 780 kpc and are not corrected for projection effects.

respective groups of old and young novae. We can see that only for 200 . . . 300″ and ∼ 700″ "bulges" there really is a significant difference on the 90% level.

In the second approach, we corrected the nova coordinates for the inclination of M 31 and computed M 31-centric distances for all objects. Of course, the effect of projection of disk novae onto the bulge must also be kept in mind here. The X-ray parameter measured for most novae is the turn-on time. Similar to Sect. 5.4, we used the connection between the WD mass and the turn-on time inferred from Hachisu & Kato (2006) to distinguish between high and low mass WDs. We defined high mass WDs as $M_{WD} \gtrsim 1.2 M_{\odot}$, which corresponds to $t_{on} \lesssim 100$d, and low mass WDs as $M_{WD} \lesssim 0.7 M_{\odot}$, corresponding to $t_{on} \gtrsim 500$d. With this selection we sampled both the high end of the WD mass distribution, which dominates the observed mass distribution of WDs in nova systems, and the region around the peak of the observed mass distribution of single WDs at $\sim 0.6 M_{\odot}$ (see Sect. 5.4). Again, we only used novae where the turn-on time is determined accurately enough. In Fig. 22 we give the distributions of the distance from the M 31 centre for both groups. It shows that novae with low mass WDs seem to be more concentrated towards the centre of the galaxy than those with high mass WDs. A KS two-sample test shows that both distributions are significantly different on the 95% level (p-value of 0.044).

It is clear that these results have to be interpreted carefully. Firstly, because of the relatively small size of the sample of SSS novae, and secondly, because of projection effects. Despite these caveats our two approaches used *two different* geometric criteria as well as *two different* X-ray parameters and reached similar results. Both approaches therefore gave a first hint that also in the X-ray regime there are two distinct populations of novae that can be associated with the different stellar environments of bulge and disk. Further observations are needed, in particular of the relatively neglected M 31 disk, in order to examine if our results can be verified.

Another observational result that we derive from Fig. 19 is that there appears to be an asymmetry in the spatial distribution of nova SSSs with respect to the major axis of M 31. There were more objects found on the (far) south-east side of M 31 than on the (near) north-west side. No such asymmetry was found in the spatial distribution with respect to the minor axis (north-east vs south-west). In Fig. 23 we plot both distributions in the upper panels and compare them in the lower panels to the equivalent distributions for all known optical novae in M 31. The overall distributions appear symmetric with respect to both axes. We carried out KS tests that confirm the visual impression. The hypothesis, that the distribution of nova SSS positions is symmetric with respect to the major axis (upper right panel in Fig. 23) is rejected on the 99% confidence level. On the other hand, the symmetry of the nova SSSs positions with respect to the minor axis (upper left panel in Fig. 23) is confirmed on the 85% level. Projection effects might influence this result slightly, but cannot explain the asymmetry.

The cause of this asymmetry might be the fact that the north-west side of the galaxy is largely seen through the gas and dust in the spiral arms of M 31 (see Walterbos & Kennicutt 1988). Bogdán & Gilfanov (2008) found a similar asymmetry for the diffuse soft X-ray emission of the M 31 bulge. Based on a microlensing survey, An et al. (2004) found that also in the optical "all the variable star distributions are asymmetric in the sense that the far side (or south-east) is brighter or has more detected objects than the near side (or north-west)". They concluded that extinction within M 31 is the reason for this behaviour. For the entire optical nova sample, we see a slight asymmetry with respect to the major axis (lower right panel in Fig. 23). The median of the distribution is shifted to the south-east (negative values in Fig. 23) by about 0.5 kpc. However, this effect is significantly weaker than the asymmetry of the nova SSSs distribution.

Therefore, we assume that extinction within M 31 is the main reason for the observed asymmetry in nova SSSs positions with respect to the major axis of M 31. Currently, the number of known nova SSSs is not sufficient to allow us to quantitatively estimate the influence of the nova position in M 31 on the SSS detection probability. Note, that such a relation, once it is derived, would be useful to implement in the simulation method described in Sect. 5.4.

6. Summary

In this paper we describe the second and third campaign of our dedicated X-ray monitoring for counterparts of classical novae in M 31 during autumn and winter 2007/8 and 2008/9. We detected in total 17 X-ray counterparts of CNe in M 31, 13 of which

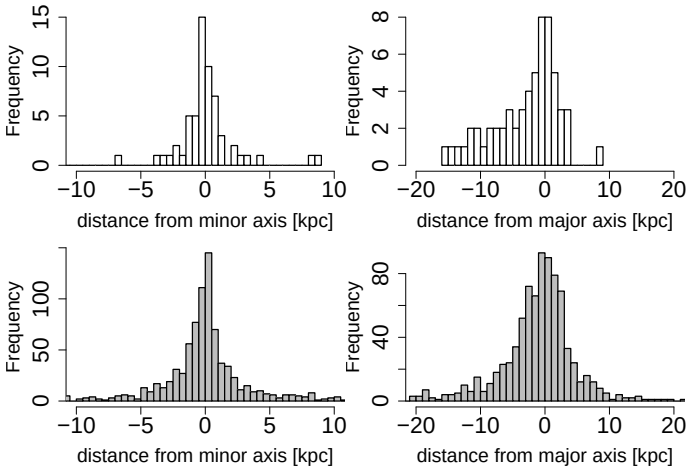

Fig. 23. Distributions of inclination corrected nova positions with respect to the minor axis (left) and the major axis (right) of M 31 for all known optical novae (lower panels, grey) and for novae with detected SSS counterpart (upper panels, white). Coordinate units are kpc, assuming a distance to M 31 of 780 kpc, and are not corrected for projection effects. Negative values correspond to positions in the south-east (near) part of M 31.

were not found in earlier studies. The remaining four novae are still active SSSs for 12.5, 11.0, 7.4 and 4.8 years after the optical outburst and it is discussed whether these long SSS phases might be sustained by re-established accretion onto the WD. During both monitoring campaigns there were only three (known) SSSs detected that do not have an optical counterpart, compared to 13 out of the 17 nova counterparts that we could classify as SSSs. Once more, this result confirms the statement of PFF2005 that novae are the major class of SSSs in the central region of M 31.

Several of the novae found in our monitoring display a short SSSs phase of less than 100 days. Based on the theoretically predicted observable WD mass distribution in novae we conducted a simulation on the detectability of nova SSS states. This simulation showed that short SSSs, which are dominating the observed nova population, could account for the high number of novae that were not detected as SSS in this and previous studies.

Based on the results from this work and previous, partly archival studies we compiled a catalogue of all novae with a SSS state in M 31 known so far. This catalogue contains in total 60 sources and for most of them several optical and X-ray parameters are known. We used this catalogue to search for statistical correlations between these properties. Relationships were found between the parameters: turn-on time, turn-off time, effective temperature kT (all X-ray), t_2 decay time and expansion velocity of the ejected envelope (both optical). We derived the values for the masses that were ejected and burned during the nova process and included them in our catalogue. Furthermore, the geometric distribution of nova SSSs in M 31 was compared with X-ray parameters. Thereby, a first hint was found that in the X-ray regime there might be two distinct populations of novae that are associated with the bulge and the disk of M 31. A similar interpretation of optical data is already the subject of discussion for almost two decades now.

It should be emphasised that the effort for a regular monitoring of M 31 dedicated to novae has led to the point were for the first time a sample of nova SSSs exists that is getting large enough to be studied with statistical methods. The trends that we derive from this sample in this work might help to gain deeper insights into the physics of the nova process. A study of nova SSSs as a population, as presented here, can only be performed in M 31. Therefore, it is important to continue the regular monitoring of this galaxy in order to examine if our first results can be confirmed with an increased sample of nova SSSs.

Acknowledgements. We are grateful to Felix Kaduk for his help in compiling the nova SSS catalogue and to Kamil Hornoch for providing us some of his unpublished nova light curves. The X-ray work is based in part on observations with XMM-Newton, an ESA Science Mission with instruments and contributions directly funded by ESA Member States and NASA. The XMM-Newton project is supported by the Bundesministerium für Wirtschaft und Technologie / Deutsches Zentrum für Luft- und Raumfahrt (BMWI/DLR FKZ 50 OX 0001) and the Max-Planck Society. M. Henze acknowledges support from the BMWI/DLR, FKZ 50 OR 0405. A.R. acknowledges support from SAO grant GO9-0024X. M. Hernanz acknowledges support from grants AYA2008-01839 and 2009-SGR-315. G.S. acknowledges support from grants AYA2008-04211-C02-01 and AYA2007-66256.

References

Alksnis, A., Smirnova, O., & Zharova, A. V. 2008, Astronomy Letters, 34, 563
An, J. H., Evans, N. W., Hewett, P., et al. 2004, MNRAS, 351, 1071
Ansari, R., Aurière, M., Baillon, P., et al. 2004, A&A, 421, 509
Baernbantner, O. & Riffeser, A. 2006, The Astronomer's Telegram, 808, 1
Balucinska-Church, M. & McCammon, D. 1992, ApJ, 400, 699
Beaton, R. L., Majewski, S. R., Guhathakurta, P., et al. 2007, ApJ, 658, L91
Bode, M. F., Darnley, M. J., Shafter, A. W., et al. 2009, ApJ, 705, 1056
Bogdán, Á. & Gilfanov, M. 2008, MNRAS, 388, 56
Brinkman, B. C., Gunsing, T., Kaastra, J. S., et al. 2000, in Society of Photo-Optical Instrumentation Engineers (SPIE) Conference Series, Vol. 4012, Society of Photo-Optical Instrumentation Engineers (SPIE) Conference Series, ed. J. E. Truemper & B. Aschenbach, 81–90
Burwitz, V., Henze, M., Pietsch, W., et al. 2008, The Astronomer's Telegram, 1364, 1
Burwitz, V., Pietsch, W., Updike, A., et al. 2007, The Astronomer's Telegram, 1238, 1
Canizares, C. R., Davis, J. E., Dewey, D., et al. 2005, PASP, 117, 1144
Capaccioli, M., Della Valle, M., Rosino, L., & D'Onofrio, M. 1989, AJ, 97, 1622
Catalán, S., Isern, J., García-Berro, E., & Ribas, I. 2008, MNRAS, 387, 1693
Ciardullo, R., Ford, H., & Jacoby, G. 1983, ApJ, 272, 92
Ciardullo, R., Ford, H. C., Neill, J. D., Jacoby, G. H., & Shafter, A. W. 1987, ApJ, 318, 520
Darnley, M. J., Bode, M. F., Kerins, E., et al. 2006, MNRAS, 369, 257
Darnley, M. J., Bode, M. F., Kerins, E., et al. 2004, MNRAS, 353, 571
Della Valle, M. 2002, in American Institute of Physics Conference Series, Vol. 637, Classical Nova Explosions, ed. M. Hernanz & J. José, 443–456
Della Valle, M., Bianchini, A., Livio, M., & Orio, M. 1992, A&A, 266, 232
Della Valle, M. & Livio, M. 1995, ApJ, 452, 704
Della Valle, M. & Livio, M. 1998, ApJ, 506, 818
Della Valle, M., Pasquini, L., Daou, D., & Williams, R. E. 2002, A&A, 390, 155
den Herder, J. W., Brinkman, A. C., Kahn, S. M., et al. 2001, A&A, 365, L7
di Mille, F., Ciroi, S., Botte, V., & Boschetti, C. S. 2003, IAU Circ., 8231, 4
Dimai, A. & Manzini, F. 2005, The Astronomer's Telegram, 421, 1
Duerbeck, H. W. 1990, in Lecture Notes in Physics, Berlin Springer Verlag, Vol. 369, IAU Colloq. 122: Physics of Classical Novae, ed. A. Cassatella & R. Viotti, 34–+
Fiaschi, M., Di Mille, F., Cariolato, R., Swift, B., & Li, W. D. 2002, IAU Circ., 7794, 1
Fiaschi, M., Tiveron, D., & Cardullo, A. 2003, IAU Circ., 8226, 2
Filippenko, A. V. & Chornock, R. 2001, IAU Circ., 7738, 3
Filippenko, A. V. & Chornock, R. 2002, IAU Circ., 7825, 3
Filippenko, A. V., Chornock, R. T., Coil, A. L., Leonard, D. C., & Li, W. D. 1999, IAU Circ., 7272, 2
Freedman, W. L., Madore, B. F., Gibson, B. K., et al. 2001, ApJ, 553, 47
Fruscione, A., McDowell, J. C., Allen, G. E., et al. 2006, in Society of Photo-Optical Instrumentation Engineers (SPIE) Conference Series, Vol. 6270, Society of Photo-Optical Instrumentation Engineers (SPIE) Conference Series
Gabriel, C., Denby, M., Fyfe, D. J., et al. 2004, in Astronomical Society of the Pacific Conference Series, Vol. 314, Astronomical Data Analysis Software and Systems (ADASS) XIII, ed. F. Ochsenbein, M. G. Allen, & D. Egret, 759–+
Greiner, J., Hasinger, G., & Kahabka, P. 1991, A&A, 246, L17
Hachisu, I. & Kato, M. 2006, ApJS, 167, 59
Hachisu, I. & Kato, M. 2010, ApJ, 709, 680
Hachisu, I., Kato, M., & Luna, G. J. M. 2007, ApJ, 659, L153

Hatano, K., Branch, D., Fisher, A., & Starrfield, S. 1997, ApJ, 487, L45
Hatzidimitriou, D., Reig, P., Manousakis, A., et al. 2007, A&A, 464, 1075
Henze, M., Burwitz, V., Pietsch, W., et al. 2007, The Astronomer's Telegram, 1336, 1
Henze, M., Burwitz, V., Pietsch, W., et al. 2008a, The Astronomer's Telegram, 1580, 1
Henze, M., Meusinger, H., & Pietsch, W. 2008b, A&A, 477, 67
Henze, M., Pietsch, W., Burwitz, V., et al. 2008c, The Astronomer's Telegram, 1602, 1
Henze, M., Pietsch, W., Haberl, F., et al. 2010, ArXiv e-prints [Paper I]
Henze, M., Pietsch, W., Haberl, F., et al. 2009a, A&A, 500, 769
Henze, M., Pietsch, W., Sala, G., et al. 2009b, A&A, 498, L13
Hernanz, M. 2005, in Astronomical Society of the Pacific Conference Series, Vol. 330, The Astrophysics of Cataclysmic Variables and Related Objects, ed. J.-M. Hameury & J.-P. Lasota, 265
Holland, S. 1998, AJ, 115, 1916
Hornoch, K. 2003, IAU Circ., 8248, 2
Hubble, E. P. 1929, ApJ, 69, 103
Immler, S., Pietsch, W., Kruse, W., et al. 2008, The Astronomer's Telegram, 1673, 1
José, J. & Hernanz, M. 1998, ApJ, 494, 680
Kaaret, P. 2002, ApJ, 578, 114
Kahabka, P., Hartmann, H. W., Parmar, A. N., & Negueruela, I. 1999, A&A, 347, L43
Kahabka, P. & van den Heuvel, E. P. J. 1997, ARA&A, 35, 69
Kong, A. K. H., Garcia, M. R., Primini, F. A., et al. 2002, ApJ, 577, 738
Krautter, J. 2002, in American Institute of Physics Conference Series, Vol. 637, Classical Nova Explosions, ed. M. Hernanz & J. José, 345
Lang, F., Lerchster, M., & Fliri, J. 2006, The Astronomer's Telegram, 821, 1
Livio, M. 1992, ApJ, 393, 516
Metropolis, N., Rosenbluth, A. W., Rosenbluth, M. N., Teller, A. H., & Teller, E. 1953, J. Chem. Phys., 21, 1087
Nedialkov, P., Orio, M., Birkle, K., et al. 2002, A&A, 389, 439
Nelson, T., Liu, J. F., di Stefano, R., et al. 2008a, The Astronomer's Telegram, 1672, 1
Nelson, T., Orio, M., Cassinelli, J. P., et al. 2008b, ApJ, 673, 1067
Ness, J., Schwarz, G., Starrfield, S., et al. 2008, AJ, 135, 1328
Ness, J., Schwarz, G. J., Retter, A., et al. 2007, ApJ, 663, 505
Orio, M. 2006, ApJ, 643, 844
Orio, M., Covington, J., & Ögelman, H. 2001, A&A, 373, 542
Orio, M. & Nelson, T. 2008, The Astronomer's Telegram, 1390, 1
Orio, M., Nelson, T., Bianchini, A., Di Mille, F., & Harbeck, D. 2010, ApJ, 717, 739
Osborne, J., Page, K., Beardmore, A., et al. 2006, The Astronomer's Telegram, 838, 1
Ovcharov, E., Valcheva, A., Kostov, A., et al. 2009, The Astronomer's Telegram, 1927, 1
Page, K. L., Osborne, J. P., Evans, P. A., et al. 2010, MNRAS, 401, 121
Payne-Gaposchkin, C. 1964, The galactic novae (New York: Dover Publication, 1964)
Petz, A., Hauschildt, P. H., Ness, J., & Starrfield, S. 2005, A&A, 431, 321
Pietsch, W., Burwitz, V., Greiner, J., et al. 2007a, The Astronomer's Telegram, 1009, 1
Pietsch, W., Burwitz, V., Greiner, J., et al. 2006a, The Astronomer's Telegram, 850, 1
Pietsch, W., Burwitz, V., Rodriguez, J., & Garcia, A. 2006b, The Astronomer's Telegram, 805, 1
Pietsch, W., Burwitz, V., Updike, A., et al. 2007b, The Astronomer's Telegram, 1257, 1
Pietsch, W., Fliri, J., Freyberg, M. J., et al. 2005a, A&A, 442, 879 [PFF2005]
Pietsch, W., Fliri, J., Freyberg, M. J., et al. 2006c, A&A, 454, 773
Pietsch, W., Freyberg, M., & Haberl, F. 2005b, A&A, 434, 483
Pietsch, W., Greiner, J., Haberl, F., & Sala, G. 2007c, The Astronomer's Telegram, 1116, 1
Pietsch, W., Haberl, F., Sala, G., et al. 2007d, A&A, 465, 375 [PHS2007]
Prialnik, D. 1986, ApJ, 310, 222
Quimby, R. 2006, The Astronomer's Telegram, 887, 1
Quimby, R., Mondol, P., Hoeflich, P., Wheeler, J. C., & Gerardy, C. 2005, The Astronomer's Telegram, 600, 1
Rau, A., Burwitz, V., Cenko, S. B., et al. 2007, The Astronomer's Telegram, 1242, 1
Rector, T. A., Jacoby, G. H., Corbett, D. L., Denham, M., & RBSE Nova Search Team. 1999, in American Astronomical Society Meeting Abstracts, Vol. 195, American Astronomical Society Meeting Abstracts, 36.08
Ries, C. . A. 2006, The Astronomer's Telegram, 829, 1
Riffeser, A., Fliri, J., Gössl, C. A., et al. 2001, A&A, 379, 362
Ritter, H., Politano, M., Livio, M., & Webbink, R. F. 1991, ApJ, 376, 177
Sala, G. & Hernanz, M. 2005, A&A, 439, 1061
Salpeter, E. E. 1955, ApJ, 121, 161
Schaefer, B. E. & Collazzi, A. C. 2010, AJ, 139, 1831
Schaefer, B. E., Pagnotta, A., Osborne, J. P., et al. 2010, The Astronomer's Telegram, 2477, 1
Schlegel, E. M., Schaefer, B., Pagnotta, A., et al. 2010, The Astronomer's Telegram, 2430, 1
Shafter, A. W. 2007a, The Astronomer's Telegram, 1341, 1
Shafter, A. W. 2007b, The Astronomer's Telegram, 1332, 1
Shafter, A. W., Coelho, E. A., Misselt, K. A., et al. 2006, The Astronomer's Telegram, 923, 1
Shafter, A. W. & Irby, B. K. 2001, ApJ, 563, 749
Shafter, A. W. & Quimby, R. M. 2007, ApJ, 671, L121
Shanley, L., Ogelman, H., Gallagher, J. S., Orio, M., & Krautter, J. 1995, ApJ, 438, L95
Sharov, A. S. & Alksnis, A. 1998, Astronomy Letters, 24, 641
Smirnova, O. & Alksnis, A. 2006, Informational Bulletin on Variable Stars, 5720, 1
Smirnova, O., Alksnis, A., & Zharova, A. V. 2006, Informational Bulletin on Variable Stars, 5737, 1
Stanek, K. Z. & Garnavich, P. M. 1998, ApJ, 503, L131
Stark, A. A., Gammie, C. F., Wilson, R. W., et al. 1992, ApJS, 79, 77
Starrfield, S. 1989, in Classical Novae, 39
Starrfield, S., Sparks, W. M., & Truran, J. W. 1974, ApJS, 28, 247
Stiele, H., Pietsch, W., Haberl, F., et al. 2010, Astronomische Nachrichten, 331, 212
Stiele, H., Pietsch, W., Haberl, F., & Freyberg, M. 2008, A&A, 480, 599
Trinchieri, G. & Fabbiano, G. 1991, ApJ, 382, 82
Trudolyubov, S. P. & Priedhorsky, W. C. 2008, ApJ, 676, 1218
Trümper, J., Hasinger, G., Aschenbach, B., Braeuninger, H., & Briel, U. G. 1991, Nature, 349, 579
Truran, J. W. & Livio, M. 1986, ApJ, 308, 721
Tuchman, Y. & Truran, J. W. 1998, ApJ, 503, 381
Valcheva, A., Ovcharov, E., Latev, G., et al. 2008, The Astronomer's Telegram, 1687, 1
van Rossum, D. R. & Ness, J. 2010, Astronomische Nachrichten, 331, 175
Voss, R., Pietsch, W., Haberl, F., et al. 2008, A&A, 489, 707
Walterbos, R. A. M. & Kennicutt, Jr., R. C. 1988, A&A, 198, 61
Warner, B. 1995, Cataclysmic variable stars (Cambridge Astrophysics Series, Cambridge, New York: Cambridge University Press, 1995)
Warner, B. 2002, in American Institute of Physics Conference Series, Vol. 637, Classical Nova Explosions, ed. M. Hernanz & J. José, 3–15
Williams, B. F., Naik, S., Garcia, M. R., & Callanan, P. J. 2006, ApJ, 643, 356
Williams, R. E. 1992, AJ, 104, 725
Wilms, J., Allen, A., & McCray, R. 2000, ApJ, 542, 914
Yaron, O., Prialnik, D., Shara, M. M., & Kovetz, A. 2005, ApJ, 623, 398